# Quantum criticality and sequential destruction of spin-orbital Kondo entanglement

Chia-Chuan Liu,[1,2] Silke Paschen,[3,1] and Qimiao Si[1]

[1] *Department of Physics and Astronomy, Rice Center for Quantum Materials, Rice University, Houston, Texas 77005, USA*
[2] *Département de Physique, Université de Montréal, Montréal, Québec, Canada H3C 3J7*
[3] *Institute of Solid State Physics, Vienna University of Technology, 1040 Vienna, Austria*

Electronic localization-delocalization has played a prominent role in realizing beyond-Landau metallic quantum critical points. It typically involves local spins induced by strong correlations. Systems that contain local multipolar moments offer new platforms to explore such quantum criticality. Here, we use an analytical method at zero temperature to study the fate of an SU(4) spin-orbital Kondo state in a multipolar Bose-Fermi Kondo model, which provides an effective description of a multipolar Kondo lattice. We show that a generic trajectory in the parameter space contains two quantum critical points, which are associated with the destruction of the Kondo entanglement in the orbital and spin channels respectively. Our asymptotically exact results reveal a global phase diagram, provides the theoretical basis for the notion of sequential Kondo destruction, and point to new forms of quantum criticality that may still be realized in a variety of strongly correlated metals.

## I. INTRODUCTION

Simple metals such as copper and aluminum are well described in terms of weakly correlated itinerant electrons. In a wide range of strongly correlated metals, the electrons' Coulomb repulsion are comparable to or larger than their bandwidth. As a result, local degrees of freedom emerge as a part of the building blocks that determine the low-energy physics[1]. A prototypical case is the magnetic heavy fermion metals, which feature many quantum phases[2–4]. Here, local spins arise from the strongly correlated $4f$-electrons. Their entanglement with the background conduction electrons gives rise to the SU(2)-symmetric Kondo effect[5], whose destruction corresponds to a localization of the $4f$-electrons and is a model case for beyond-Landau quantum critical points (QCPs)[6–13].

The combination of the strong correlations, large spin-orbit coupling and suitable crystalline symmetry can also produce multipolar moments. Because they couple with each other and with conduction electrons in new ways, these multipolar systems not only provide a setting to demonstrate the robustness of the notion that local degrees of freedom influence metallic quantum criticality, but also allow for the realization of even richer forms of QCPs. For the Kondo effect *per se*, various kinds of local degrees of freedom have led to a variety of Kondo states relevant to multipolar heavy fermion metals[14–21], multi-orbital iron-based compounds[22–25], synthetic systems such as ultracold atoms[26] and mesoscopic devices[27–29], and other correlated settings[30–33].

Experimentally, there is a growing list of heavy fermion metals in which the role of multipolar degrees of freedom has been explored on their quantum criticality[1,34]. These include $Pr(TM)_2Al_{20}$(TM = Ti, V), which have non-magnetic doublets in the ground-state manifold[35,36], $PrOs_4Sb_{12}$, which involves field-induced local quadrupolar moments[37,38], and $YbRu_2Ge_2$, which hosts quasi-degenerate spin and higher-rank moments[39,40].

Of direct interest to us is $Ce_3Pd_{20}Si_6$, which has recently been investigated as a function of a non-thermal control parameter (magnetic field)[41,42]. The results show two stages of Kondo-destruction quantum criticality. In this system, the $4f$ electrons form a total angular momentum $J = 5/2$ state whose six-fold degeneracy is further split as dictated by the point-group symmetry[43]. What lies in the ground-state manifold is the $\Gamma_8$ quartet[44], which can be represented in the pseudo-spin $\vec{\sigma}$ and pseudo-orbital $\vec{\tau}$ bases (see Appendix). The competition between the Kondo entanglement in the $\Gamma_8$-manifold and the associated RKKY interactions may therefore be responsible for this sequential Kondo destruction.

Extensive efforts have already been devoted to the study of multipolar Kondo effects *per se*, as already described. What the experimental developments call for is the understanding of the competition between the multipolar Kondo couplings to the conduction electrons and collective fluctuations of the multipolar moments, a topic that has remains largely unexplored. The striking experimental observations in $Ce_3Pd_{20}Si_6$ motivate a well-defined theoretical question: what is the generic type of QCPs that result from this type of competition? The minimal model of interest, put forward in Ref. 41, is the spin-orbital entwined multipolar Bose-Fermi Kondo model (BFK) illustrated in Fig. 1. It is an effective model that emerges in the extended dynamical mean field theory of the multipolar Kondo lattice (see Appendix). The

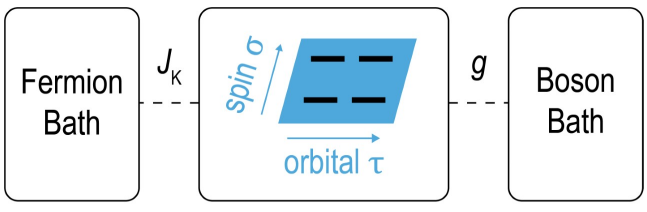


FIG. 1. Illustration of the spin-orbital-entwined multipolar Bose-Fermi Kondo model (1)

model involves the local degrees of freedom, containing both the spin $\sigma$ and the orbital $\tau$ components, which are coupled to the fermionic and bosonic baths. The former couplings describe the (fermionic) Kondo effect, while the latter describes the collective fluctuations associated with the RKKY interactions. An earlier study using a continuous-time quantum Monte Carlo method indicated split quantum phase transitions[41]. The numerical study left open the question of whether a generic tuning trajectory leads to split transitions or whether it could also involve a one-stage transition.

In this work, we study the multipolar Bose-Fermi Kondo model at zero temperature. By using a Coulomb-gas representation of the Bose-Fermi Kondo model, we carry out analytical renormalization-group (RG) calculations that are controlled by an expansion in terms of a small quantity $\epsilon$ (defined in Eq. 3). Our asymptotically exact theory is able to uncover a global phase diagram at zero temperature, which reveals the mechanism for the sequential Kondo destruction and shows that it appears for any generic trajectory in the phase diagram.

### A. Summary of the main result

To summarize our result more specifically, we visualize it in terms of an overall phase diagram presented in the $g_{\sigma z}$-$g_{\tau z}$ parameter space, as illustrated in Fig. 2. Here, $g_{\sigma z}$ and $g_{\tau z}$ are the couplings of the local multipolar moment to the bosonic fields in the spin and orbital channels, respectively. The fermionic Kondo couplings that are kept fixed.

Our main results are as follows:

- In the special case with the spin and orbital bosonic couplings being equal, $g_{\sigma z} = g_{\tau z}$, we identify a critical fixed point that is accessible by the $\epsilon$-expansion. This critical point, marked by the red point in Fig. 2, describes a one-stage transition for the destruction of the SU(4) spin-orbital Kondo effect.

- We find the anisotropy between these two bosonic couplings are relevant in the RG sense. This implies that the one-stage Kondo-destruction cannot describe the quantum phase transition along a generic trajectory in the phase diagram.

- Moreover, we are able to determine the complete phase diagram asymptotically exactly, as shown in Fig. 2. This is made possible by realizing that all the phase boundaries meet at the equal-bosonic-coupling critical fixed point, near which the run-away RG flows are still small within the $\epsilon$-expansion. It is further substantiated by a more comprehensive RG analysis presented in Appendices (C) and (D).

The global phase diagram implies two stages of Kondo-destruction QCPs for *any* generic tuning trajectory at zero temperature, one each in the spin and orbital channels despite their entwining in the Hamiltonian. This is illustrated by the sequence of quantum phase transitions along the solid black lines in Fig. 2. As such, our asymptotically-exact results provide the theoretical basis for the notion of sequential Kondo destruction that has been implicated by the experiments in $Ce_3Pd_{20}Si_6$ and the associated numerical studies[41]. Given the various forms of multipolar and related Kondo effects[14,15,27,29], our results open the door towards new forms of quantum criticality that may still be realized in a rich variety of strongly correlated metals.

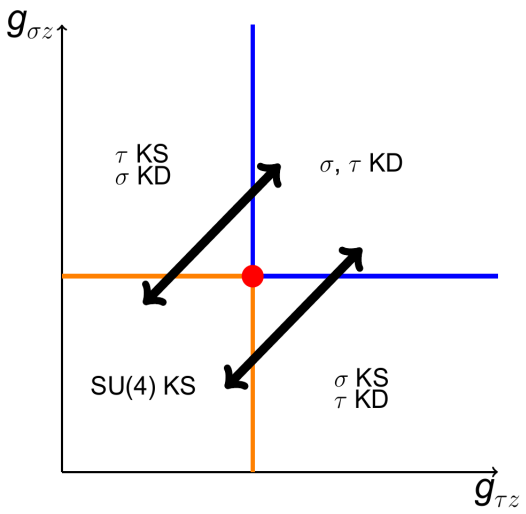


FIG. 2. The global phase diagram of the model (1), presented in the $g_{\sigma z}$-$g_{\tau z}$ parameter space for fixed Kondo couplings. Here, KD and KS refer to the phases with Kondo-destruction and Kondo screening, respectively, whereas $\sigma$ and $\tau$ refer to spin and orbital, respectively. The black arrows mark generic trajectories in the parameter space that correspond to the tuning of a non-thermal physical control parameter. The global phase diagram implies two-stages of Kondo destruction along any generic tuning trajectory.

The rest of the paper is organized as follows. In Sec. II, we specify the spin-orbial-entwined Bose-Fermi-Kondo model. Sec. III presents the RG analysis in a fine-tuned case, which sets the stage for the analysis in the generic cases that is given in Sec. IV. The resulting global phase diagram is presented in Sec. V. We relegate the additional details of the model to Appendices (A) and (B), and the description of a comprehensive RG analysis to Appendices (C) and (D).

## II. MODEL AND SOLUTION METHODS

In this section, we specify the model and describe the setup for our asymptotically exact analysis.

### A. The multipolar Bose-Fermi Kondo model

The multipolar Bose-Fermi Kondo model is given by the following Hamiltonian:

$$H_{BFK} = H_0 + H_{K,0} + H_{BK} \ . \tag{1}$$

Here, $H_0$ is the non-interacting part for the conduction electron $c_{p,i\alpha}$ and the bosonic baths $\vec{\phi}\kappa, q$ (where $\kappa = \sigma, \tau, m$):

$$\begin{aligned} H_0 = &\sum_{p,i\alpha} \epsilon_p c^\dagger_{p,i\alpha} c_{p,i\alpha} \\ &+ \sum_q W_q \left( \vec{\phi}^\dagger_{\sigma,q} \cdot \vec{\phi}_{\sigma,q} + \vec{\phi}^\dagger_{\tau,q} \cdot \vec{\phi}_{\tau,q} + \vec{\phi}^\dagger_{m,q} \cdot \vec{\phi}_{m,q} \right) \ . \end{aligned} \tag{2}$$

To set up controlled RG calculation, we introduce an expansion parameter $\epsilon$, which is defined through the bosonic spectral function $W_q$:

$$\sum_q \left[ \delta\left(\omega - W_q\right) + \delta\left(\omega + W_q\right) \right] = \left( \frac{K_0^2}{\pi} \right) |\omega|^{1-\epsilon} \operatorname{sgn} \omega \ , \tag{3}$$

with $0 < \epsilon < 1$, and for $|\omega| < \Lambda$, which specifies a high-energy cut-off scale.

The fermionic Kondo coupling between the local multipolar moment and conduction electrons is as follows:

$$H_{K,0} = \left[ J_\sigma \vec{\sigma} \cdot \vec{\sigma}_c + J_\tau \vec{\tau} \cdot \vec{\tau}_c + 4 J_M \left( \vec{\sigma}_i \otimes \vec{\tau} \right) \cdot \left( \vec{\sigma}_c \otimes \vec{\tau}_c \right) \right] \ , \tag{4}$$

where $\vec{\sigma}\left(\vec{\tau}\right)$ and $\vec{\sigma}_c\left(\vec{\tau}_c\right)$ are the spin (orbital) operators of the single impurity and the conduction electron, respectively. The spin and orbital operators of the conduction electrons are defined as:

$$\begin{aligned} \vec{\sigma}_c &= \frac{1}{2} \sum_{i,\alpha\beta} c^\dagger_{i\alpha} \vec{s}_{\alpha\beta} c_{i\beta} \ , \\ \vec{\tau}_c &= \frac{1}{2} \sum_{ij,\alpha} c^\dagger_{i\alpha} \vec{t}_{ij} c_{j\alpha} \ , \\ \vec{\sigma} \otimes \vec{\tau}_c &= \frac{1}{4} \sum_{ij,\alpha\beta} c^\dagger_{i\alpha} \vec{s}_{\alpha\beta} \otimes \vec{t}_{ij} c_{j\beta} \ . \end{aligned} \tag{5}$$

Here, we use $\alpha, \beta$ and $i, j$ to denote the spin and orbital indices, respectively. Thus, $\vec{s}_{\alpha\beta}$ and $\vec{t}_{ij}$ are Pauli matrices in the spin and orbital subspaces, respectively. For the fermionic Kondo Hamiltonian alone, the anisotropy in the couplings is generically unimportant as the system restores the SU(4) symmetry in the Kondo-entangled ground state[5]. We have therefore chosen the bare Kondo Hamiltonian to be SU(2) symmetric in the spin as well as in the orbital sector, with an overall SU(2)⊗SU(2) symmetry. The full renormalized Kondo Hamiltonian (C3) for the later RG analysis is shown in Appendix (C).

Finally, the coupling between the local multipolar moment and the bosonic bath is given by:

$$H_{BK} = g_{\sigma z} \sigma_z \phi_{\sigma z} + g_{\tau z} \tau_z \phi_{\tau z} + g_m \left( \sigma_z \otimes \tau_z \right) \phi_m \ , \tag{6}$$

where $\vec{\phi}_\kappa = \sum_q \left( \vec{\phi}_{\kappa,q} + \vec{\phi}^\dagger_{\kappa,-q} \right)$ with $\kappa = \sigma, \tau, m$. We focus on the Ising-anisotropic case for the couplings in both the spin and orbital channels ($g_{\sigma z}$ and $g_{\tau z}$, respectively) as well as for the spin-orbital mixed coupling ($g_m$).

The BFK model $H_{BFK}(1)$ is mapped from a multipolar Kondo lattice model that contains a lattice of local levels with a four-fold degeneracy by the scheme of extended dynamical mean field theory[45–47].

### B. Setting up the RG analysis

In spite of the entwining of the spin and orbital degrees of freedom, we are able to establish results that are asymptotically exact and with a simple structure. In this subsection, we set the stage to tackle this rich problem using the (asymptotically exact) RG approach. Further details can be found in the Appendix.

First, our goal is to study the generic phase diagram in the $g_{\sigma z}$-$g_{\tau z}$ parameter space. In other words, we fix the fermionic Kondo couplings and vary $g_{\sigma z}$ and $g_{\tau z}$. For this purpose, it suffices to keep the mixed bosonic coupling $g_m = 0$. A non-vanishing but small $g_m$ does not modify the structure of the phase diagram, as we show in Appendix (E). To proceed, we use a bosonization approach to represent the BFK model (1) in terms of a Coulomb gas, from which a controlled RG calculation based on an expansion in $\epsilon$ is possible[48–50].

Second, the Ising couplings of $H_{BK}$ (6) break not only the SU(4) symmetry but also the smaller SU(2)×SU(2) symmetry. While the Kondo couplings in $H_K$ respect the SU(2)×SU(2) symmetry, under the RG flow these couplings will generically become spin anisotropic. It turns out that one needs to consider five types of Kondo couplings. Together with the spin and orbital Ising couplings $g_{\sigma z}$ and $g_{\tau z}$ of $H_{BK}$ (6), the total number of RG coupling constants is seven. The large number of the RG charges makes it a challenge to determine the overall RG flow structure. We are able to accomplish this goal by analyzing the problem in several steps.

Crucially, we take the first step to be a fine-tuned trajectory in the phase diagram. Recall that the $g_{\sigma z}$-$g_{\tau z}$ parameter space is of our interest. For clarity, we visualize this parameter space in Fig. 3(a), which marks the relevant phases. The fine-tuned trajectory we focus our initial analysis on corresponds to identical couplings to the bosonic baths in the spin and orbital sectors. It goes along the diagonal in the $g_{\sigma z}$-$g_{\tau z}$ space, and is marked as trajectory "I" in Fig. 3(a). The result of the analysis on this fine-tuned trajectory provides a anchoring point, which allows us to determine the sequence of quantum phase transitions along generic trajectories of the phase diagram.

We note that it is possible to rigorously establish the phase diagram, Fig. 3(a), through a comprehensive RG analysis without taking the fund-tuned trajectory "I" as the starting anchoring point. This is described in Appendices (C) and (D). We choose to present the step-by-step

analysis here in the main text, given that it reveals the underlying physics in a considerably more transparent way.

## III. QUANTUM PHASE TRANSITIONS: FINE-TUNED CASE

We now turn to the RG calculation of the spin-orbital coupled Bose-Fermi Kondo model (1). As outlined in the previous section, we will start from trajectory "I" of Fig 3(a), which corresponds to the fine-tuned case of equal bosonic couplings in the spin and orbital channels, $g_{\sigma z} = g_{\tau z}$. We demonstrate a critical point (marked by the red solid point in Fig 3(a)) that is accessible by an $\epsilon$-expansion in our RG analysis. It describes a direct transition from the spin and orbital Kondo-destroyed (KD) phase to the fully ( spin or orbital) Kondo-screened (KS) phase. It will be shown in the next section that, by analyzing the vicinity of this critical point, we can determine the structure of the overall phase diagram.

As we have mentioned, generally the total number of coupling constants is seven. However, under the trajectory $g_{\sigma z} = g_{\tau z} = g$, some of the coupling constants are irrelevant, or can be combined due to the symmetry constraint, and thus the numbers of relevant RG equations (the $\beta$ functions) is substantially reduced. We leave the details in appendix D 2, and only show the final reduced $\beta$ functions:

$$\begin{aligned} \frac{dy_1}{dl} &= (1-2M)\, y_1 + 2y^2 \\ \frac{dy}{dl} &= (1-M)\, y + 2y_1 y \\ \frac{dM}{dl} &= \left(\epsilon - 4y_1^2 - 4y^2\right) M \end{aligned} \tag{7}$$

where $y \propto J_{\sigma\perp} = J_{\tau\perp}$ flips either spin or orbital indices, $M \propto g_{\sigma z}^2 = g_{\tau z}^2 = g^2$, and $y_1 \propto J_{M1}$ is the part of the Kondo coupling $J_M$ that flips both the spin and orbital indices (See Eq. (C3) in appendix C). Note that we can set $J_{\sigma\perp} = J_{\tau\perp}$, given that we are considering a path in the parameter space that preserves the symmetry $\sigma \leftrightarrow \tau$.

From these reduced $\beta$ functions (7), we identify a critical point $(y_1^*, y^*, M^*) = \left(\frac{-1+\sqrt{1+12\epsilon}}{12}, \frac{\sqrt{-1+12\epsilon+\sqrt{1+12\epsilon}}}{6\sqrt{2}}, \frac{5+\sqrt{1+12\epsilon}}{6}\right) \cong \left(0, \frac{\sqrt{\epsilon}}{2}, 1\right)$ (up to the order $\sqrt{\epsilon}$). This fixed point has one relevant direction with the scaling dimension $\sqrt{2\epsilon}$ and separates the spin and orbital KD phase ($y_1 \to 0, y \to 0, M \to \infty$) from the SU(4) KS phase ($y_1 \to \infty, y \to \infty, M \to 0$)[51]. The RG flow structure of the reduced $\beta$ functions (7) is plotted in Fig. 3(b). For latter convenience, we name SU(4) KS phase as **K3**, and the critical point (the red dot in Fig. 3(b) as **R1**.

Because **R1** is accessible by the $\epsilon$-expansion, we can address what happens in the vicinity of this fixed point.

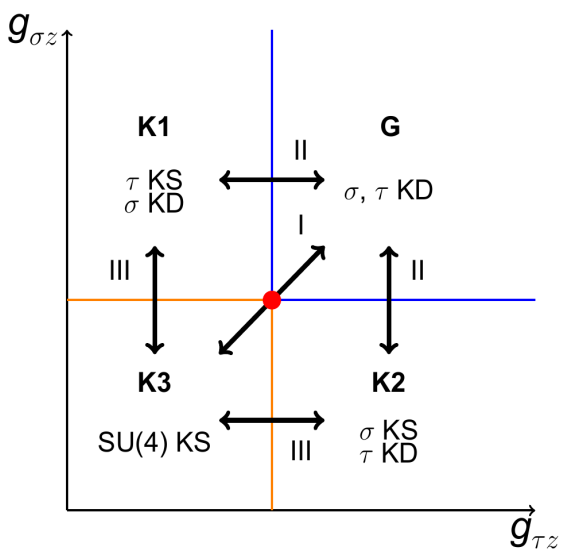


(a)

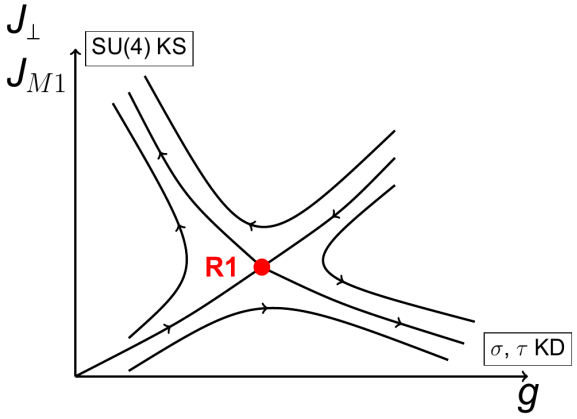


(b)

FIG. 3. (a) Trajectories in the parameter space of the BFK model (1), marked as "I"-"III", along which the RG analyses are carried out in steps. The labels "G", "K1", "K2" and "K3" describe the RG fixed points for the corresponding phases. (b) RG flow diagram of the reduced $\beta$ functions (7), where $g = g_{\sigma z} = g_{\tau z}$. "**R1**" marks the unstable fixed point that captures the transition along the fine-tuned trajectory "I" of (a).

We will show in the next section that any small asymmetry between $g_{\tau z}$ and $g_{\sigma z}$ around **R1** is relevant in the RG sense. As a result, the direct phase transition between spin and orbital KD phase and SU(4) KS phase is fine-tuned. In other words, this direct transition occurs at a point in the parameter space – the red dot in Fig. 3(a) and 3(a) – instead of through a boundary line.

For our analysis, one feature of the fixed point **R1** plays a crucial role. While the fixed-point value for the RG charge $M$ is O(1), the values for the RG charges (the fugacities) $y_1$ and $y$ are of order $\sqrt{\epsilon}$. Because of this fea-

ture, the quardratic-in-$y_\alpha$ terms in the beta-functions of the fugacities turn out to be unimportant for both RG flow structure and the leading order of the scaling dimensions. The same conclusion is also seen in the scaling dimensions of the RG variables near **R1**; to the leading non-vanishing order in $\epsilon$, they are the same regardless of whether the quardratic-in-$y_\alpha$ terms are kept in the beta-functions of the fugacities. In the next section, we'll see how this allows us to determine the overall structure of the phase diagram by expanding the RG equations around the fixed point **R1**. In particular, it allows us to carry out a complete analysis of the quantum phase transition along trajectory "III", which otherwise would have been much harder to achieve.

## IV. QUANTUM PHASE TRANSITIONS: GENERIC CASES

So far we have considered the case of equal bosonic couplings in the spin and orbital channels, *i.e.*, $g_{\sigma z} = g_{\tau z} = g$. However, these two couplings are generically different. Thus, we have to determine the quantum phase transitions along trajectories away from the diagonal in the $g_{\sigma z}$-$g_{\tau z}$ parameter space. We find that there are two sets of trajectories, which are marked by "II" and "III" in Fig. 3(a). We describe our analyses of these two case in turn.

### A. Transition to spin or orbital Kondo-entangled phase

We next consider the transition between the spin and orbital KD phase and the spin or orbital KS phase. Importantly, we do so by starting from the RG trajectory around the critical point **R1** where $g_{\sigma z} = g_{\tau z} = g^*$ between the spin and orbital KD and the SU(4) KS phases. As we have just alluded to, around **R1**, any small asymmetry between $g_{\tau z}$ and $g_{\sigma z}$ is relevant with the scaling dimension $\sqrt{2\epsilon}$(up to the order $\sqrt{\epsilon}$) in RG sense,.

Suppose we slightly increase the coupling constant $g_{\sigma z}$,

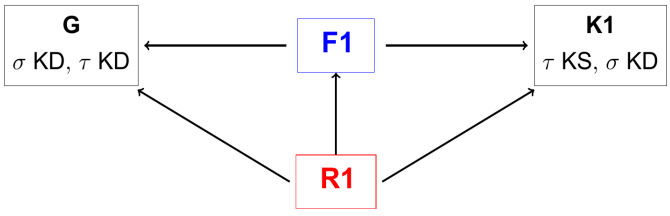


FIG. 4. The schematic RG flow structure of the phase transition between the orbital and spin KD phase and the spin KS phase denoted as **G** and **K1**, respectively. Around the multi-critical point **R1**, once the $g_{\sigma z}$ is slightly enlarged, the RG trajectory will flow toward **F1**, which is the generic critical point separating **G** and **K1**.

while keeping all the parameters fixed. In other words, now $g_{\sigma z} > g_{\tau z} = g^*$. The RG trajectory will flow towards $g_{\sigma z} \to \infty$. We can then vary $g_{\tau z}$ to map out the RG flow.

The corresponding trajectories in the phase diagram are denoted as arrow (II) in Fig. 3(a). Along this trajectory, the reduced $\beta$ functions are:

$$\begin{aligned} \frac{dy_2}{dl} &= (1 - M^\sigma)\, y_2 \\ \frac{dM^\sigma}{dl} &= \left(\epsilon - 4y_2^2\right) M^\sigma \end{aligned} \tag{8}$$

where $y_2 \propto J_{\sigma\perp}$ flips only the orbital indices, and $M^\sigma \propto g_{\sigma z}^2$. Again, we leave the details of the derivation in Appendix D 3.

From the reduced $\beta$ functions (8), one can identify another critical fixed point $(y_2^*, M^{\sigma *}) = \left(\frac{\sqrt{\epsilon}}{2}, 1\right)$. This fixed point has one relevant direction with scaling dimension $\sqrt{2\epsilon}$ (up to the order $\sqrt{\epsilon}$) and separates the spin KS phase $(y_2 \to \infty, M^\sigma \to 0)$ from the spin and orbital KD phase $(y_2 \to 0, M^\sigma \to \infty)$.

The schematic RG flow structure is shown in Fig. 4, where the spin and orbital KD phase and the spin KS phase, denoted as **G** and **K1**, respectively, are separated by the critical point denoted as **F1**. Based on this RG structure, we establish the transition between the spin and orbital KD phase and the spin KS phase. By applying a precisely parallel analysis, we establish the phase transition between spin and orbital KD phase and the orbital KS phase; we name the associated critical point as **F2**.

### B. Transition between spin or orbital KS phase and SU(4) KS phase

We have so far analyzed the transitions out of the spin and orbital KD phase. This phase can transit into the spin or orbital KS phase without fine-tuning the parameters. It can also transit into the SU(4) KS phase by fine-tuning the parameters.

Because the spin or orbital KS phase and the SU(4) KS phase correspond to different stable strong coupling fixed points, there must be other generic critical points that separate them. These generic critical points describe the phase transition between the spin or orbital KS phase and the SU(4) KS phase, as shown in the phase diagram trajectory denoted as the dashed arrow (III) in Fig. 3(a). In this section, we would like to finally establish the transition between the spin or orbital KS phase and the SU(4) KS phase, which correspond to the trajectories (III) in Fig. 3(a).

Again, we focus on the RG trajectory around the critical point **R1** where $g_{\sigma z} = g_{\tau z} = g^*$ between the spin and orbital KD and SU(4) KS phases. If we keep every parameters fixed but just slightly decrease the coupling constant $g_{\sigma z}$, that is, $g_{\sigma z} < g_{\tau z} = g^*$, then the RG trajectory will flow toward to $g_{\sigma z} \to 0$. We can then vary

$g_{\tau z}$ to explore the RG trajectory. The corresponding trajectories in the phase diagram are denoted as the arrow III in Fig. 3(a).

However, unlike **R1** and **F1**, the real locations of the **X1** is harder to identify directly from the $\beta$ functions. To proceed, we exploit the property of the critical point **R1** that we alluded to earlier: Here, all of the fugacity $y \sim \sqrt{\epsilon}$ around **R1**. Near **R1**, one can thus neglect the higher order terms of $\sqrt{\epsilon}$ in the $\beta$ functions of the fugacity (See Appendix (D 4) for more details), and in the end the final reduced $\beta$ functions are

$$\begin{aligned} \frac{dy_1}{dl} &= (1 - M^\tau)\, y_1 \\ \frac{dy_3}{dl} &= (1 - M^\tau)\, y_3 \\ \frac{dM^\tau}{dl} &= \left(\epsilon - 4y_1^2 - 4y_3^2\right) M^\tau \end{aligned} \tag{9}$$

where $y_3 \propto J_{\tau\perp}$.

From the reduced $\beta$ functions (9), one can identify a critical line $(y_1^*, y_3^*, M^{\tau *}) = \left(a, \frac{\sqrt{\epsilon - 4a^2}}{2}, 1\right)$ where $a$ is a constant, which separates the spin and orbital KS phase from the spin KS phase and corresponds to the critical point **X1** in Fig. 5 with scaling dimension $\sqrt{2\epsilon}$. By a parallel analysis, the transition between the spin and orbital KS phase and the orbital KS phase can also be established.

## V. PHASE DIAGRAM AND THE SEQUENTIAL KONDO DESTRUCTION

Based on the above, we have established the global phase diagram, which is shown in Fig. 2. This phase diagram is also seen through a complete RG flow, Fig. 3(a), which combines the RG flows along the various trajectories we have described in the previous sections. [A complementary, and more comprehensive, way of deriving this complete RG flow is given in Appendix (D).] We summarize the characterization of the various phases and their transitions as follows:

- The boxes **K1**-**K3** are different kinds of strong Kondo coupling fixed points, and the box **G** is the spin and orbital KD fixed point. These fixed points are all stable according to the $\beta$ functions (C39), and thus describe phases of matter.

- The red box **R1** is a multi-critical point between the spin and orbital KD phase and SU(4) KS phase since there are two relevant directions around it.

- The blue boxed **F1**-**F2** are generic critical point separating different types the spin and orbital KD phases to either spin or orbital KS phases.

- Because the strong Kondo coupling fixed points **K1**, **K2**, and **K1** are stable fixed points, t they are separated by the generic critical points **X1** and **X2**. The generic critical points **X1** and **X2** control the critical phenomena of the trajectories III in Fig. 3(a).

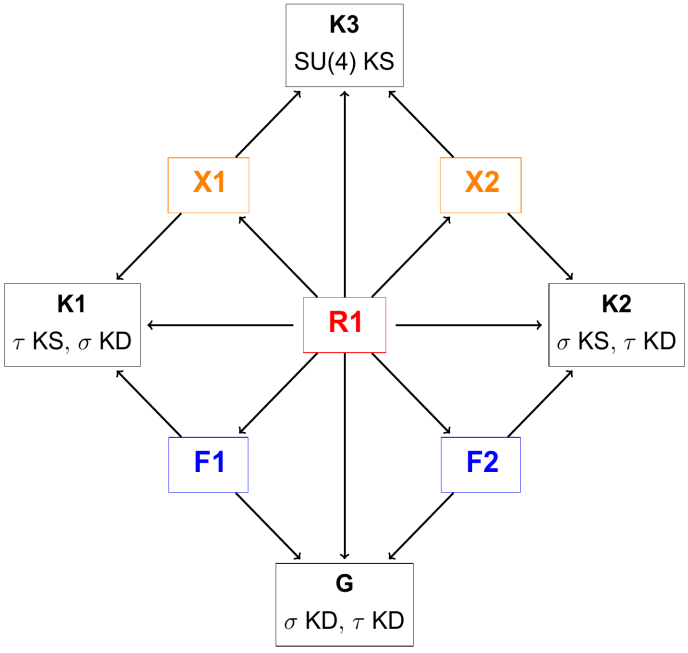


FIG. 5. The schematic structure of the fixed points and the relative RG flow of the BFK model (1), as derived from the RG analysis. Here KS and KD is the abbreviation for the Kondo-screened and the Kondo-destroyed fixed point, respectively. The boxes **K1**-**K3** are different kinds of strong Kondo coupling fixed points, and the box **G** is the spin and orbital KD fixed point. The red box **R1** is a multi-critical point between spin and orbital KD phase and SU(4) KS phase. The blue boxed **F1**-**F2** are generic critical point separating different types the spin and orbital KD phases to either spin or orbital KS phases. Because the strong Kondo coupling fixed points **K1**, **K2**, and **K3** are stable fixed points, they are separated by the generic critical points, denoted as orange boxes **X1** and **X2**.

The solid black arrows in Fig. 2 marks the generic tuning trajectories in the zero-temperature phase diagram. Along each of such trajectories, two-stages of Kondo destruction take place, each characterizing a QCP in the spin or orbital channel. This asymptotically exact result provides a firm theoretical basis to understand the field-induced quantum phase transitions that have been experimentally observed in $Ce_3Pd_{20}Si_6$.

## VI. SUMMARY AND OUTLOOK

In this work, we have performed a detailed renormalization-group analysis of a spin-orbital-entwined Bose-Fermi-Kondo model, which is mapped from a multipolar Kondo lattice model. We are able to determine the global phase diagram at zero temperature, which re-

veals the mechanism for the sequential Kondo destruction and shows that it appears for any generic trajectory in the phase diagram. As such, our results provide a firm theoretical basis for understanding the surprising experimental results in the heavy fermion metal $Ce_3Pd_{20}Si_6$.

More generally, our work elucidates the quantum criticality in spin-orbital-coupled heavy fermion systems. Our results also make it clear how multipolar degrees of freedom, which entwine different types of quantum numbers such as spins and orbitals, allows for new types of Kondo-driven quantum criticality. Because the cooperation of strong correlations, large spin-orbit coupling and crystalline symmetry represents a robust means to create varied local degrees of freedom, our study opens up a new avenue to design novel types of beyond-Landau quantum criticality.


## ACKNOWLEDGMENTS

We thank Ang Cai, Kevin Ingersent, Emilian Nica and Rong Yu for useful discussions. The work has been supported in part by the NSF Grant No. DMR-1920740 and the Robert A. Welch Foundation Grant No. C-1411. Work in Vienna has been supported by the Austrian Science Fund (P29296 and 29279) and the European Community (H2020 Project No. 824109). One of us (Q.S.) acknowledges the hospitality of the Aspen Center for Physics, which is supported by the NSF grant No. PHY-1607611.


## Appendix A: The case of $Ce_3Pd_{20}Si_6$

In $Ce_3Pd_{20}Si_6$, every $Ce^{3+}$ ion contributes one localized 4f electron. Because of the strong spin-orbit coupling, the spin and orbital degree of freedom of the 4f electron are coupled to together into a total angular momentum $J = 5/2$ state that has six-fold degeneracy and hence supports not only dipole moment but also higher-order multipolar moments. Such six-fold degeneracy is split into a $\Gamma_8$ quartet and a $\Gamma_7$ doublet due to the crystal field effect[43]. The analysis of temperature dependent inelastic neutron scattering and entropy data also revealed that the $\Gamma_8$ quartet is the true ground state for the local levels[44], which can be represented in the pseudo-spin $\vec{\sigma}$ and pseudo-orbital $\vec{\tau}$ notation as:

$$\begin{aligned}
|\tau_z = 1; \sigma_z = 1\rangle &= \sqrt{\frac{5}{6}}|J_z = \frac{5}{2}\rangle + \sqrt{\frac{1}{6}}|J_z = -\frac{3}{2}\rangle \\
|\tau_z = 1; \sigma_z = -1\rangle &= \sqrt{\frac{1}{6}}|J_z = \frac{5}{2}\rangle + \sqrt{\frac{5}{6}}|J_z = -\frac{3}{2}\rangle \\
|\tau_z = -1; \sigma_z = 1\rangle &= |J_z = \frac{1}{2}\rangle \\
|\tau_z = -1; \sigma_z = -1\rangle &= |J_z = -\frac{1}{2}\rangle
\end{aligned} \tag{A1}$$

The $\Gamma_8$ systems comprise dipoles, quadrupoles, and octupoles, all of which are irreducible representations of the $O_h$ group of the cubic lattice. Both dipolar (magnetic) and quadrupolar order (and likely even octupolar order) may arise via the RKKY interaction between the local multipolar moments[43].

Applying a magnetic field leads to a sequence of two QCPs, which are associated with the magnetic and quadrupolar degrees of freedom respectively[41]. Across each QCP, a jump of the Hall coefficient is found based on extrapolation of its isothermal dependence to the zero-temperature limit[41]. Each jump implicates a destruction of Kondo effect and the concomitant electronic localization-delocalization phase transition at zero temperature.

## Appendix B: Multipolar Kondo lattice model

To demonstrate how multiple stages of Kondo destruction can arise without fine-tuning the parameters, we start from a multipolar Kondo lattice model that contains a lattice of local levels with a four-fold degeneracy which can be expressed in term of spin $\vec{\sigma}$ and orbital $\vec{\tau}$ operators:

$$H_{KL} = H_c + H_l + H_K. \tag{B1}$$

The first part $H_c = \sum_{\vec{k}\sigma\tau} \epsilon_{\vec{k}\sigma\tau} c^\dagger_{\vec{k}\sigma\tau} c_{\vec{k}\sigma\tau}$ defines the kinetic energy of the conduction electrons, and the second part $H_f$ describes the RKKY interaction among the $\Gamma_8$ local levels. For the purpose of convenience and demonstration, we choose $H_l$ as the Ising type:

$$H_l = \sum_{ij} \left[ I^{\sigma}_{ij} \sigma^z_i \sigma^z_j + I^{\tau}_{ij} \tau^z_i \tau^z_j + I^{m}_{ij} \left( \sigma^z_i \otimes \tau^z_i \right) \left( \sigma^z_j \otimes \tau^z_j \right) \right] \tag{B2}$$

where, $\vec{\sigma}$, $\vec{\tau}$, and $\vec{\sigma} \otimes \vec{\tau}$ express the spin and orbital operators and their tensor product, respectively, and $I^{\sigma}_{ij}, I^{\tau}_{ij}, I^{m}_{ij}$ are the corresponding coupling constant. Note that here the English letter $i, j$ are indices for sites. The Hamiltonian is essentially the Ising anisotropic version of the Kugel-Khomskii model.

The final part $H_K$ is the Kondo coupling between the local levels and their conduction-electron counterparts:

$$H_K = \sum_i \left[ J_{\sigma} \vec{\sigma}_i \cdot \vec{\sigma}_{i,c} + J_{\tau} \vec{\tau}_i \cdot \vec{\tau}_{i,c} + 4 J_M \left( \vec{\sigma}_i \otimes \vec{\tau}_i \right) \cdot \left( \vec{\sigma}_{i,c} \otimes \vec{\tau}_{i,c} \right) \right] \tag{B3}$$

where the antiferromagnetic Kondo coupling $J_{\kappa} > 0$ with $\kappa = \sigma, \tau, M$, respectively, describe the interaction of the local levels $\vec{\sigma}$, $\vec{\tau}$, and $\vec{\sigma} \otimes \vec{\tau}$ with the conduction-electron counterparts.

The multipolar Bose-Fermi Kondo model $H_{BFK}$ (1) is mapped from the multipolar Kondo lattice model $H_{KL}$ (B1) under the extended dynamical mean field theory[45–47]. In this procedure, all the sites except for a local impurity are traced out, and the effect of the RKKY interactions between the local multipolar moments is to act effectively as a self-consistent bosonic bath that, along with the self-consistent fermionic bath, are coupled to the local impurity.

## Appendix C: Derivation of the Coulomb gas action and RG equations

As we mentioned in the main text, because of the Ising-type couplings

$$H_{BK} = g_{\sigma z} \sigma_z \phi_{\sigma z} + g_{\tau z} \tau_z \phi_{\tau z} \tag{C1}$$

, the whole Bose-Fermi Kondo model (1) breaks not only the SU(4) symmetry but also the SU(2)×SU(2) symmetry. Therefore, to perform the RG calculation, one need to reduce the symmetry in the Kondo part $H_K$ and introduce much more Kondo couplings. To our purpose, the model with the minimal number of parameters that we need to consider is:

$$H_{BFK} = H_0 + H_{K,o} + H_{BK} \tag{C2}$$

where $H_0$ is the non-interacting part for the conduction electron $c_{p,i\alpha}$ and the bosonic bath $\vec{\phi}_{\kappa,q} (\kappa = \sigma, \tau, m)$, and the Kondo coupling $H_{K,o}$ is

$$\begin{aligned} H_{K,o} &= J_{\sigma z} \sigma^z \sigma^z_c + J_{\sigma \perp} \left( \sigma^x \sigma^x_c + \sigma^y \sigma^y_c \right) + J_{\tau z} \tau^z \tau^z_c + J_{\tau \perp} \left( \tau^x \tau^x_c + \tau^y \tau^y_c \right) \\ &+ 4 J_{M1} \left[ \left( \sigma_x \otimes \tau_x \right) \left( \sigma_x \otimes \tau_x \right)_c + \left( \sigma_x \otimes \tau_y \right) \left( \sigma_x \otimes \tau_y \right)_c + \left( \sigma_y \otimes \tau_x \right) \left( \sigma_y \otimes \tau_x \right)_c + \left( \sigma_y \otimes \tau_y \right) \left( \sigma_y \otimes \tau_y \right)_c \right] \\ &+ 4 J_{M2} \left[ \left( \sigma_z \otimes \tau_x \right) \left( \sigma_z \otimes \tau_x \right)_c + \left( \sigma_z \otimes \tau_y \right) \left( \sigma_z \otimes \tau_y \right)_c \right] + 4 J_{M3} \left[ \left( \sigma_x \otimes \tau_z \right) \left( \sigma_x \otimes \tau_z \right)_c + \left( \sigma_y \otimes \tau_z \right) \left( \sigma_y \otimes \tau_z \right)_c \right] \\ &+ 4 J_{M4} \left[ \left( \sigma_z \otimes \tau_z \right) \left( \sigma_z \otimes \tau_z \right)_c \right] \end{aligned} \tag{C3}$$

with $J_{\sigma \perp} = J_{M3}$ and $J_{\tau \perp} = J_{M2}$. Note that compared with the coupling with bosnic bath (6), we had already set $g_m = 0$ in the coupling (C1). In Appendix (E) We will also show that a non-vanishing but small $g_m$ does not modify the structure of our phased diagram based on the RG analysis.

Note that, without the bosonic coupling (6), both the Hamiltonian (1) and (C2) admit only a SU(4) Kondo-screened fixed point. In addition, as we will see, tuning the bosonic coupling (C1) breaks the SU(4) Kondo-screened fixed point directly down to either a spin or orbital SU(2) Kondo-screened fixed point. Therefore, one should expect that how the bare Kondo couplings deviate from the SU(4) symmetric case does not really matter, and the RG analysis of the model (C2) captures the generic phase diagram of model (1).

For the Ising-type bosonic coupling, to perform a controllable RG calculation, one need to map the Bose-Fermi Kondo model into a Coulomb gas type model[48,49]. The first step to decompose the above Hamiltonian $H_{BFK}$ into the part $H_0$ that is diagonal in the space of the single impurity states $|\sigma\rangle \otimes |\tau\rangle$, and the other part $H_f$ that is not:

$$H_{BFK} = H_D + H_f \tag{C4}$$

where $H_D$ is diagonal in the space of the single impurity states $|\sigma\rangle \otimes |\tau\rangle$. We use the notation $|m\rangle = |i\alpha\rangle$ to denote a single impurity state with the orbital $i = 1, 2$ and the spin $\alpha = \uparrow, \downarrow$. Therefore,

$$H_D = \sum_m H_m |m\rangle\langle m| \tag{C5}$$

Then we rewrite $H_m$ in term of the projection operators $X_{mm} = |m\rangle\langle m| = |i\alpha\rangle\langle i\alpha|$, so that:

$$\begin{aligned} H_m &= E_m + \sum_n V_m^n c_n^\dagger c_n + \sum_{k,n} E_k c_{k,n}^\dagger c_{k,n} + \sum_q W_q \left( \vec{\phi}_{\sigma,q}^\dagger \cdot \vec{\phi}_{\sigma,q} + \vec{\phi}_{\tau,q}^\dagger \cdot \vec{\phi}_{\tau,q} \right) \\ &+ \sum_q F_\sigma^m \left( \phi_{\sigma z,q} + \phi_{\sigma z,-q}^\dagger \right) + \sum_q F_\tau^m \left( \phi_{\tau z,q} + \phi_{\tau z,-q}^\dagger \right) \end{aligned} \tag{C6}$$

where

$$\begin{aligned} V_{i\alpha}^{i\alpha} &= \frac{1}{4} \left( J_{\sigma z} + J_{\tau z} + J_{M4} \right) \\ V_{i\alpha}^{i\overline{\alpha}} &= \frac{1}{4} \left( J_{\tau z} - J_{\sigma z} - J_{M4} \right) \\ V_{i\alpha}^{\bar{i}\alpha} &= \frac{1}{4} \left( J_{\sigma z} - J_{\tau z} - J_{M4} \right) \\ V_{i\alpha}^{\bar{i}\overline{\alpha}} &= -\frac{1}{4} \left( J_{\sigma z} + J_{\tau z} - J_{M4} \right) \end{aligned} \tag{C7}$$

and

$$\begin{aligned} F_\sigma^{i\uparrow} &= g_{\sigma z} \\ F_\sigma^{i\downarrow} &= -g_{\sigma z} \\ F_\tau^{1\alpha} &= g_{\tau z} \\ F_\tau^{2\alpha} &= -g_{\tau z} \end{aligned} \tag{C8}$$

Here we use the over-line symbol to denote the complement of the spin or orbital index.

On the other hand, the flipping part is defined as:

$$H_f = \sum_{m \neq n} Q\left(m, n\right) \tag{C9}$$

where

$$Q\left(m, m\right) = |m\rangle\langle m| H_f |n\rangle\langle n| \tag{C10}$$

describing the process of flipping from the single impurity state $|n\rangle$ to $|m\rangle$. Specifically,

$$\begin{aligned} Q\left(i\alpha, \bar{i}\overline{\alpha}\right) &= J_{M1} c_{\bar{i}\overline{\alpha}}^\dagger c_{i\alpha} |i\alpha\rangle\langle \bar{i}\overline{\alpha}| \\ Q\left(i\alpha, i\overline{\alpha}\right) &= \frac{1}{2} \left( J_{\sigma\perp} - J_{M3} \right) c_{\bar{i}\overline{\alpha}}^\dagger c_{\bar{i}\alpha} |i\alpha\rangle\langle i\overline{\alpha}| + \frac{1}{2} \left( J_{\sigma\perp} + J_{M3} \right) c_{i\overline{\alpha}}^\dagger c_{i\alpha} |i\alpha\rangle\langle i\overline{\alpha}| = J_{\sigma\perp} c_{i\overline{\alpha}}^\dagger c_{i\alpha} |i\alpha\rangle\langle i\overline{\alpha}| \\ Q\left(i\alpha, \bar{i}\alpha\right) &= \frac{1}{2} \left( J_{\tau\perp} - J_{M2} \right) c_{\bar{i}\overline{\alpha}}^\dagger c_{i\overline{\alpha}} |i\alpha\rangle\langle \bar{i}\alpha| + \frac{1}{2} \left( J_{\tau\perp} + J_{M2} \right) c_{\bar{i}\alpha}^\dagger c_{i\alpha} |i\alpha\rangle\langle \bar{i}\alpha| = J_{\tau\perp} c_{\bar{i}\alpha}^\dagger c_{i\alpha} |i\alpha\rangle\langle \bar{i}\alpha| \end{aligned} \tag{C11}$$

since $J_{\sigma\perp} = J_{M3}$ and $J_{\tau\perp} = J_{M2}$.

Since $H_D$ is diagonal in the single impurity states, after tracing out these local states, the partition function can be expanded in $H_f$, and the results is:

$$Z = \sum_{n=0}^{\infty} \int_0^\beta d\tau_n ... \int_0^{\tau_{i+1}} d\tau_i ... \int_0^{\tau_2} d\tau_1 \sum_m A\left(m; \tau_n, ..., \tau_1\right) \tag{C12}$$

Here the transition amplitude is defined as:

$$\begin{aligned} A\left(m; \tau_n, ...\tau_1\right) &= (-1)^n \sum_{m_2, ..., m_n} \int DcD\phi \exp\left[-H_m\left(\beta - \tau_n\right)\right] Q'\left(m, m_n\right) \times ... \\ &\times \exp\left[-H_{m_{i+1}}\left(\tau_{i+1} - \tau_i\right)\right] Q'\left(m_{i+1}, m_i\right) \exp\left[-H_{m_i}\left(\tau_i - \tau_{i-1}\right)\right] \times ... \\ &\times \exp\left[-H_{m_2}\left(\tau_2 - \tau_1\right)\right] Q'\left(m_2, m\right) \exp\left[-H_m \tau_1\right] \end{aligned} \tag{C13}$$

where

$$Q'\left(m_{i+1},m_i\right)=\langle m_{i+1}|H_f|m_i\rangle \tag{C14}$$

, which can be separated as:

$$\langle m|H_f|n\rangle=y'_{m,n}O'\left(m,n\right) \tag{C15}$$

with

$$\begin{aligned}
y'_{i\alpha,\bar{i\overline{\alpha}}}&=J_{M1}\\
y'_{i\alpha,i\overline{\alpha}}&=\frac{1}{2}\left(J_{\sigma\perp}+J_{M3}\right)=J_{\sigma\perp}\\
y'_{i\alpha,\bar{i}\alpha}&=\frac{1}{2}\left(J_{\tau\perp}+J_{M2}\right)=J_{\tau\perp}\\
O'_{i\alpha,\bar{i\overline{\alpha}}}&=c^{\dagger}_{\bar{i\overline{\alpha}}}c_{i\alpha}\\
O'_{i\alpha,i\overline{\alpha}}&=c^{\dagger}_{i\overline{\alpha}}c_{i\alpha}\\
O'_{i\alpha,i\overline{\alpha}}&=c^{\dagger}_{\bar{i}\alpha}c_{i\alpha}
\end{aligned} \tag{C16}$$

Now we can trace out the conduction electron by using the bosonization technique. For our single impurity problem, we only need to consider the s-wave component:

$$c_{i\alpha}\left(x\right)=\frac{1}{\sqrt{2\pi a}}e^{-i\theta_{i\alpha}(x)} \tag{C17}$$

The projected Hamiltonian thus transforms into:

$$H_m=H_c+H_{\phi_\sigma}+H_{\phi_\tau}+E'_m+\sum_n\frac{\delta^n_m}{\pi\rho_0}\left(\frac{d\theta_n\left(x\right)}{dx}\right)+\sum_q F^m_\sigma\left(\phi_{\sigma z}+\phi^{\dagger}_{\sigma z,-q}\right)+\sum_q F^m_\tau\left(\phi_{\tau z,q}+\phi^{\dagger}_{\tau z,-q}\right) \tag{C18}$$

where $E'_m=E_m+\Delta E_m$, $\rho_0$ is the bare conduction electron density of state, and $\delta^{j\beta}_{i\alpha}$ is the phase shift from the scattering potential:

$$\begin{aligned}
\delta^{i\alpha}_{i\alpha}&=\tan^{-1}\left(\pi\rho_0V^{i\alpha}_{i\alpha}\right)=\tan^{-1}\left[\frac{\pi\rho_0}{4}\left(J_{\sigma z}+J_{\tau z}+J_{M4}\right)\right]\\
\delta^{i\overline{\alpha}}_{i\alpha}&=\tan^{-1}\left(\pi\rho_0V^{i\overline{\alpha}}_{i\alpha}\right)=\tan^{-1}\left[\frac{\pi\rho_0}{4}\left(J_{\tau z}-J_{\sigma z}-J_{M4}\right)\right]\\
\delta^{\bar{i}\alpha}_{i\alpha}&=\tan^{-1}\left(\pi\rho_0V^{\bar{i}\alpha}_{i\alpha}\right)=\tan^{-1}\left[\frac{\pi\rho_0}{4}\left(J_{\sigma z}-J_{\tau z}-J_{M4}\right)\right]\\
\delta^{\bar{i\overline{\alpha}}}_{i\alpha}&=\tan^{-1}\left(\pi\rho_0V^{\bar{i\overline{\alpha}}}_{i\alpha}\right)=\tan^{-1}\left[-\frac{\pi\rho_0}{4}\left(J_{\sigma z}+J_{\tau z}-J_{M4}\right)\right]
\end{aligned} \tag{C19}$$

The history dependent potential is treated then through introducing a canonical transformation at each imaginary time:

$$U_\delta=\exp\left(i\frac{\delta}{\pi}\theta\right) \tag{C20}$$

The potential after the canonical transformation is time-independent because of the property:

$$U^{\dagger}_\delta H_cU_\delta=H_c+\frac{\delta}{\pi\rho_0}\frac{d\theta}{dx} \tag{C21}$$

We also introduce a similar canonical transformation to the bosonic degree of freedom,

$$\begin{aligned}
U_{W_{\sigma,m}}&=\exp\left(\sum_q\frac{F^m_\sigma}{W_q}\left(\phi_{\sigma z,q}-\phi^{\dagger}_{\sigma z,-q}\right)\right)\\
U_{W_{\tau,m}}&=\exp\left(\sum_q\frac{F^m_\tau}{W_q}\left(\phi_{\tau z,q}-\phi^{\dagger}_{\tau z,-q}\right)\right)
\end{aligned} \tag{C22}$$

with the property:

$$\begin{aligned} U_{W_{\sigma,m}}^{\dagger} H_{\phi_\sigma} U_{W_{\sigma,m}} &= H_{\phi_\sigma} + \sum_q F_\sigma^m \left(\phi_{\sigma z,q} + \phi_{\sigma z,-q}^{\dagger}\right) \\ U_{W_{\tau,m}}^{\dagger} H_{\phi_\tau} U_{W_{\tau,m}} &= H_{\phi_\tau} + \sum_q F_\tau^m \left(\phi_{\tau z,q} + \phi_{\tau z,-q}^{\dagger}\right) \end{aligned} \tag{C23}$$

The transition amplitude now reduce to:

$$\begin{aligned} A\left(m;\tau_n,...,\tau_1\right) &= Z_c \sum_{m_{n+1}=\alpha_1=m,m_2,...m_{n-1}} y'_{m_{n+1},\alpha_n}...y'_{m_{i+1},m_i}...y'_{m_2,m_1} \\ &\times \exp\left[-E'_m\left(\tau_1-\tau_n\right) - \sum_{i=2}^{n-1} E'_{m_{i+1}}\left(\tau_{i+1}-\tau_i\right)\right] \\ &\times \left\langle O\left(m_{n+1},m_n\right)\left(\tau_n\right)...O\left(m_{i+1},m_i\right)\left(\tau_i\right)...O\left(m_2,m_1\right)\left(\tau_1\right)\right\rangle \\ &\times \left\langle B_\sigma\left(m_{n+1},m_n\right)\left(\tau_n\right)...B_\tau\left(m_{i+1},m_i\right)\left(\tau_i\right)...B_\sigma\left(m_2,m_1\right)\left(\tau_1\right)\right\rangle \\ &\times \left\langle B_\tau\left(m_{n+1},m_n\right)\left(\tau_n\right)...B_\tau\left(m_{i+1},m_i\right)\left(\tau_i\right)...B_\tau\left(m_2,m_1\right)\left(\tau_1\right)\right\rangle \end{aligned} \tag{C24}$$

Here, for the bosonic part

$$\begin{aligned} B_\sigma\left(m_{i+1},M_i\right)\left(\tau_i\right) &= U_{W_{\sigma,m_{i+1}}} U_{W_{\sigma,m_i}}^{\dagger}\left(\tau_i\right) \\ B_\tau\left(m_{i+1},m_i\right)\left(\tau_i\right) &= U_{W_{\tau,m_{i+1}}} U_{W_{\tau,m_i}}^{\dagger}\left(\tau_i\right) \end{aligned} \tag{C25}$$

, the correlation function can be reduced into

$$\begin{aligned} &\left\langle B_\sigma\left(m_{n+1},m_n\right)\left(\tau_n\right)...B_\sigma\left(m_2,m_1\right)\left(\tau_1\right)\right\rangle = U_{W_{\sigma,m_{i+1}}} U_{W_{\sigma,m_i}}^{\dagger}\left(\tau_i\right) \\ &= \left\langle \prod_i \exp\left(-\sum_q \frac{F_{\sigma z}^{m_{i+1}m_i}}{W_q}\left(\phi_{\sigma z,q} - \phi_{\sigma z,-q}^{\dagger}\right)\left(\tau_i\right)\right)\right\rangle \\ &= \left\langle \exp\left(\sum_{ij} C_\sigma\left(\tau_i-\tau_j\right)\exp\left(\Delta_E\right)\right)\right\rangle \end{aligned} \tag{C26}$$

and similarly

$$\begin{aligned} &\left\langle B_\tau\left(m_{n+1},m_n\right)\left(\tau_n\right)...B_\tau\left(m_2,m_1\right)\left(\tau_1\right)\right\rangle \\ &= U_{W_{\tau,m_{i+1}}} U_{W_{\tau,m_i}}^{\dagger}\left(\tau_i\right) = \left\langle \prod_i \exp\left(-\sum_q \frac{F_{\tau z}^{m_{i+1}m_i}}{W_q}\left(\phi_{\tau z,q} - \phi_{\tau z,-q}^{\dagger}\right)\left(\tau_i\right)\right)\right\rangle \\ &= \left\langle \exp\left(\sum_{ij} C_\tau\left(\tau_i-\tau_j\right)\exp\left(\Delta_E\right)\right)\right\rangle \end{aligned} \tag{C27}$$

where

$$\begin{aligned} F_\sigma^{m_{i+1}m_i} &= F_\sigma^{m_{i+1}} - F_\sigma^{m_i} \\ C_\sigma\left(\tau_i-\tau_j\right) &= \sum_q \frac{F_\sigma^{m_{i+1}m_i} F_\sigma^{m_{j+1}m_j}}{W_q^2}\exp\left(-W_q\left(\tau_j-\tau_i\right)\right) \end{aligned} \tag{C28}$$

and

$$\begin{aligned} F_\tau^{m_{i+1}m_i} &= F_\tau^{m_{i+1}} - F_\tau^{m_i} \\ C_\tau\left(\tau_i-\tau_j\right) &= \sum_q \frac{F_\tau^{m_{i+1}m_i} F_\tau^{m_{j+1}m_j}}{W_q^2}\exp\left(-W_q\left(\tau_j-\tau_i\right)\right) \end{aligned} \tag{C29}$$

with

$$\sum_q \exp\left(-W_q\tau\right) = \frac{K_0}{\tau^{2-\epsilon}} \tag{C30}$$

On the other hand, for the conduction electron part

$$O\left(m_{i+1}, m_i\right)\left(\tau_i\right) = \exp\left(H_c\tau_i\right) O\left(m_{i+1}, m_i\right) \exp\left(-H_c\tau_i\right) \tag{C31}$$

Here,

$$O\left(m_{i+1}, m_i\right) = \left(\prod_n U_{\delta^n_{m_{i+1}}}\right) O'\left(m, m_i\right) \left(\prod_n U^\dagger_{\delta^n_{n_i}}\right) \tag{C32}$$

and for different channels, they are:

$$\begin{aligned}
O\left(i\alpha, \bar{i}\overline{\alpha}\right) &= \prod_{j\beta} U^{j\beta}_{i\alpha} c^\dagger_{\bar{i}\overline{\alpha}} c_{i\alpha} \prod_{j\beta} U^{\dagger j\beta}_{\bar{i}\overline{\alpha}} \\
&= \exp\left[\left(\frac{\delta^{i\alpha}_{i\alpha}}{\pi} - \frac{\delta^{i\alpha}_{\bar{i}\overline{\alpha}}}{\pi} - 1\right)\theta_{i\alpha} + \left(\frac{\delta^{i\overline{\alpha}}_{i\alpha}}{\pi} - \frac{\delta^{i\overline{\alpha}}_{\bar{i}\overline{\alpha}}}{\pi}\right)\theta_{i\overline{\alpha}} + \left(\frac{\delta^{\bar{i}\alpha}_{i\alpha}}{\pi} - \frac{\delta^{\bar{i}\alpha}_{\bar{i}\overline{\alpha}}}{\pi}\right)\theta_{\bar{i}\alpha} + \left(\frac{\delta^{\bar{i}\overline{\alpha}}_{i\alpha}}{\pi} - \frac{\delta^{\bar{i}\overline{\alpha}}_{\bar{i}\overline{\alpha}}}{\pi} + 1\right)\theta_{\bar{i}\overline{\alpha}}\right] \\
O\left(i\alpha, i\overline{\alpha}\right) &= \prod_{j\beta} U^{j\beta}_{i\alpha} c^\dagger_{i\overline{\alpha}} c_{i\alpha} \prod_{j\beta} U^{\dagger j\beta}_{i\overline{\alpha}} \\
&= \exp\left[\left(\frac{\delta^{i\alpha}_{i\alpha}}{\pi} - \frac{\delta^{i\alpha}_{i\overline{\alpha}}}{\pi} - 1\right)\theta_{i\alpha} + \left(\frac{\delta^{i\overline{\alpha}}_{i\alpha}}{\pi} - \frac{\delta^{i\overline{\alpha}}_{i\overline{\alpha}}}{\pi} + 1\right)\theta_{i\overline{\alpha}} + \left(\frac{\delta^{\bar{i}\alpha}_{i\alpha}}{\pi} - \frac{\delta^{\bar{i}\alpha}_{i\overline{\alpha}}}{\pi}\right)\theta_{\bar{i}\alpha} + \left(\frac{\delta^{\bar{i}\overline{\alpha}}_{i\alpha}}{\pi} - \frac{\delta^{\bar{i}\overline{\alpha}}_{i\overline{\alpha}}}{\pi}\right)\theta_{\bar{i}\overline{\alpha}}\right] \\
O\left(i\alpha, \bar{i}\alpha\right) &= \prod_{j\beta} U^{j\beta}_{i\alpha} c^\dagger_{\bar{i}\alpha} c_{i\alpha} \prod_{j\beta} U^{\dagger j\beta}_{\bar{i}\alpha} \\
&= \exp\left[\left(\frac{\delta^{i\alpha}_{i\alpha}}{\pi} - \frac{\delta^{i\alpha}_{\bar{i}\alpha}}{\pi} - 1\right)\theta_{i\alpha} + \left(\frac{\delta^{i\overline{\alpha}}_{i\alpha}}{\pi} - \frac{\delta^{i\overline{\alpha}}_{\bar{i}\alpha}}{\pi}\right)\theta_{i\overline{\alpha}} + \left(\frac{\delta^{\bar{i}\alpha}_{i\alpha}}{\pi} - \frac{\delta^{\bar{i}\alpha}_{\bar{i}\alpha}}{\pi} + 1\right)\theta_{\bar{i}\alpha} + \left(\frac{\delta^{\bar{i}\overline{\alpha}}_{i\alpha}}{\pi} - \frac{\delta^{\bar{i}\overline{\alpha}}_{\bar{i}\alpha}}{\pi}\right)\theta_{\bar{i}\overline{\alpha}}\right]
\end{aligned} \tag{C33}$$

We can rewrite these term as:

$$O\left(m, n\right) = \exp\left[i\sum_r e^r_{mn}\theta_r\right] \tag{C34}$$

After all of these, the partition function is mapped into:

$$\frac{Z}{Z_0} = \sum_{n=0}^{\infty} \sum_{m_{n+1}=m_1=m, m_2, \ldots m_{n-1}} \int_{\xi_0}^{\beta-\xi_0} \frac{d\tau_n}{\xi_0} \ldots \int_{\xi_0}^{\tau_{i+1}-\xi_0} \frac{d\tau_i}{\xi_0} \ldots \int_{\xi_0}^{\tau_2-\xi_0} \frac{d\tau_1}{\xi_0} \exp\left[-S\left(\tau_1, \ldots, \tau_n\right)\right] \tag{C35}$$

with a Coulomb gas type action:

$$\begin{aligned}
S\left(\tau_1, \ldots, \tau_n\right) &= -\sum_i \ln y_{m_i, m_{i+1}} + \sum_i h_{m_{i+1}} \frac{\tau_{i+1} - \tau_i}{\xi_0} \\
&+ \sum_{i<j} \left[K_{m_i, m_j} + K_{m_{i+1}, m_{j+1}} - K_{m_i, m_{j+1}} - K_{m_{i+1}, m_j}\right] \ln \frac{\tau_j - \tau_i}{\xi_0} \\
&- \sum_{i<j} \left[M^\sigma_{m_i, m_j} + M^\sigma_{m_{i+1}, m_{j+1}} - M^\sigma_{m_i, m_{j+1}} - M^\sigma_{m_{i+1}, m_j}\right] \left[\left(\frac{\tau_j - \tau_i}{\xi_0}\right)^\epsilon - 1\right] \\
&- \sum_{i<j} \left[M^\tau_{m_i, m_j} + M^\tau_{m_{i+1}, m_{j+1}} - M^\tau_{m_i, m_{j+1}} - M^\tau_{m_{i+1}, m_j}\right] \left[\left(\frac{\tau_j - \tau_i}{\xi_0}\right)^\epsilon - 1\right]
\end{aligned} \tag{C36}$$

where $h_m \propto E'_m$, $\xi_0$ is the ultraviolet cutoff, and

$$\begin{aligned} y_{m,n} &= y'_{m,n}\xi_0 \\ K_{m,n} &= -\frac{1}{2}\sum_r \left(e^r_{mn}\right)^2 \\ M^\sigma_{m,n} &= -\frac{1}{2}\sum_q \left(F^{mn}_\sigma\right)^2 \\ M^\tau_{m,n} &= -\frac{1}{2}\sum_q \left(F^{mn}_\tau\right)^2 \end{aligned} \tag{C37}$$

By following these definitions, for the Bose-Fermi Kondo model (C2) the non-vanishing fugacity $y_{m,n}$ and stiffness $K_{m,n}$, $M^\sigma_{m,n}$ and $M^\tau_{m,n}$ are:

$$\begin{aligned} y_{i\alpha,\bar{i}\bar{\alpha}} &\equiv y_1 = \xi_0 J_{M1} \\ y_{i\alpha,i\bar{\alpha}} &\equiv y_2 = \xi_0 J_{\sigma\perp} \\ y_{i\alpha,\bar{i}\alpha} &\equiv y_3 = \xi_0 J_{\tau\perp} \\ K_{i\alpha,\bar{i}\bar{\alpha}} &\equiv -K_1 = -f_1\left(J_{\sigma z}, J_{\tau z}, J_{M4}\right) \\ K_{i\alpha,i\bar{\alpha}} &\equiv -K_2 = -f_2\left(J_{\sigma z}, J_{\tau z}, J_{M4}\right) \\ K_{i\alpha,\bar{i}\alpha} &\equiv -K_3 = -f_3\left(J_{\sigma z}, J_{\tau z}, J_{M4}\right) \\ M^\sigma_{i\alpha,\bar{i}\bar{\alpha}} &= M^\sigma_{i\alpha,i\bar{\alpha}} \equiv -M^\sigma = -\Gamma\left(\epsilon\right) g^2_{\sigma z} \\ M^\tau_{i\alpha,\bar{i}\bar{\alpha}} &= M^\tau_{i\alpha,\bar{i}\alpha} \equiv -M^\tau = -\Gamma\left(\epsilon\right) g^2_{\tau z} \end{aligned} \tag{C38}$$

where $\Gamma\left(\epsilon\right)$ is a $\epsilon$ dependent O(1) constant. The explicit expression of $K_{1,2,3}$ is complicated but unnecessary, and can be derived from Eq. (C33), where the phase shifts are known in Eq. (C19). The only few things that matter are that they depend only on indices-preserving coupling $J_{\sigma z,\tau z,M4}$, and the range of their bare value is $f_{1,2,3}\left(J_{\sigma z}, J_{\tau z}, J_{M4}\right) \in (0,3)$.

For the Coulomb gas action (C36), the associated $\beta$ equations can be derived through a conventional manner[49,50,52–54], and it turns out:

$$\begin{aligned} \frac{dy_1}{dl} &= \left(1 - K_1 - M^\sigma - M^\tau\right) y_1 + 2y_2 y_3 \\ \frac{dy_2}{dl} &= \left(1 - K_2 - M^\sigma\right) y_2 + 2y_1 y_3 \\ \frac{dy_3}{dl} &= \left(1 - K_3 - M^\tau\right) y_3 + 2y_1 y_2 \\ \frac{dK_1}{dl} &= -2y_1^2\left(2K_1\right) - 2y_2^2\left(K_1 + K_2 - K_3\right) - 2y_3^2\left(K_1 + K_3 - K_2\right) \\ \frac{dK_2}{dl} &= -2y_1^2\left(K_2 + K_1 - K_3\right) - 2y_2^2\left(2K_2\right) - 2y_3^2\left(K_2 + K_3 - K_1\right) \\ \frac{dK_3}{dl} &= -2y_1^2\left(K_3 + K_1 - K_2\right) - 2y_2^2\left(K_3 + K_2 - K_1\right) - 2y_3^2\left(2K_3\right) \\ \frac{dM^\sigma}{dl} &= \left(\epsilon - 4y_1^2 - 4y_2^2\right) M^\sigma \\ \frac{dM^\tau}{dl} &= \left(\epsilon - 4y_1^2 - 4y_3^2\right) M^\tau \end{aligned} \tag{C39}$$

## Appendix D: RG analysis and the generic phase diagram

In this section, we give a detailed RG analysis of the $\beta$ functions (C39). We will identify the fixed points of the $\beta$ functions (C39) by using $\epsilon$ as the control parameter. The relative stability of these fixed points are analysed through

the eigenvalues and eigenvectors of the matrix:

$$W = \begin{pmatrix} \frac{\partial \beta_{y_1}}{\partial y_1} & \frac{\partial \beta_{y_1}}{\partial y_2} & \frac{\partial \beta_{y_1}}{\partial y_3} & \frac{\partial \beta_{y_1}}{\partial K_1} & \frac{\partial \beta_{y_1}}{\partial K_2} & \frac{\partial \beta_{y_1}}{\partial K_3} & \frac{\partial \beta_{y_1}}{\partial M^\sigma} & \frac{\partial \beta_{y_1}}{\partial M^\tau} \\ \frac{\partial \beta_{y_2}}{\partial y_1} & \frac{\partial \beta_{y_2}}{\partial y_2} & \frac{\partial \beta_{y_2}}{\partial y_3} & \frac{\partial \beta_{y_2}}{\partial K_1} & \frac{\partial \beta_{y_2}}{\partial K_2} & \frac{\partial \beta_{y_2}}{\partial K_3} & \frac{\partial \beta_{y_2}}{\partial M^\sigma} & \frac{\partial \beta_{y_2}}{\partial M^\tau} \\ \frac{\partial \beta_{y_3}}{\partial y_1} & \frac{\partial \beta_{y_3}}{\partial y_2} & \frac{\partial \beta_{y_3}}{\partial y_3} & \frac{\partial \beta_{y_3}}{\partial K_1} & \frac{\partial \beta_{y_3}}{\partial K_2} & \frac{\partial \beta_{y_3}}{\partial K_3} & \frac{\partial \beta_{y_3}}{\partial M^\sigma} & \frac{\partial \beta_{y_3}}{\partial M^\tau} \\ \frac{\partial \beta_{K_1}}{\partial y_1} & \frac{\partial \beta_{K_1}}{\partial y_2} & \frac{\partial \beta_{K_1}}{\partial y_3} & \frac{\partial \beta_{K_1}}{\partial K_1} & \frac{\partial \beta_{K_1}}{\partial K_2} & \frac{\partial \beta_{K_1}}{\partial K_3} & \frac{\partial \beta_{K_1}}{\partial M^\sigma} & \frac{\partial \beta_{K_1}}{\partial M^\tau} \\ \frac{\partial \beta_{K_2}}{\partial y_1} & \frac{\partial \beta_{K_2}}{\partial y_2} & \frac{\partial \beta_{K_2}}{\partial y_3} & \frac{\partial \beta_{K_2}}{\partial K_1} & \frac{\partial \beta_{K_2}}{\partial K_2} & \frac{\partial \beta_{K_2}}{\partial K_3} & \frac{\partial \beta_{K_2}}{\partial M^\sigma} & \frac{\partial \beta_{K_2}}{\partial M^\tau} \\ \frac{\partial \beta_{K_3}}{\partial y_1} & \frac{\partial \beta_{K_3}}{\partial y_2} & \frac{\partial \beta_{K_3}}{\partial y_3} & \frac{\partial \beta_{K_3}}{\partial K_1} & \frac{\partial \beta_{K_3}}{\partial K_2} & \frac{\partial \beta_{K_3}}{\partial K_3} & \frac{\partial \beta_{K_3}}{\partial M^\sigma} & \frac{\partial \beta_{K_3}}{\partial M^\tau} \\ \frac{\partial \beta_{M^\sigma}}{\partial y_1} & \frac{\partial \beta_{M^\sigma}}{\partial y_2} & \frac{\partial \beta_{M^\sigma}}{\partial y_3} & \frac{\partial \beta_{M^\sigma}}{\partial K_1} & \frac{\partial \beta_{M^\sigma}}{\partial K_2} & \frac{\partial \beta_{M^\sigma}}{\partial K_3} & \frac{\partial \beta_{M^\sigma}}{\partial M^\sigma} & \frac{\partial \beta_{M^\sigma}}{\partial M^\tau} \\ \frac{\partial \beta_{M^\tau}}{\partial y_1} & \frac{\partial \beta_{M^\tau}}{\partial y_2} & \frac{\partial \beta_{M^\tau}}{\partial y} & \frac{\partial \beta_{M^\tau}}{\partial K_1} & \frac{\partial \beta_{M_3^\tau}}{\partial K_2} & \frac{\partial \beta_{M^\tau}}{\partial K_3} & \frac{\partial \beta_{M^\tau}}{\partial M^\sigma} & \frac{\partial \beta_{M^\tau}}{\partial M^\tau} \end{pmatrix} \tag{D1}$$

,

We will also illustrate the generic phase diagram Fig. 3(a) based on our RG analysis.

### 1. RG analysis

In the $\epsilon$ expansion, the $\epsilon$ serve as a small control parameter. We will express the fixed point in term of the $\epsilon$ up to the leading order $\sqrt{\epsilon}$. By solving the zeros of the $\beta$ functions (C39), the fixed points can be identified:

$$\begin{aligned} &\mathbf{R1}: \ y_1 = 0, \ y_2 = y_3 = \frac{\sqrt{\epsilon}}{2}, \ K_1 = K_2 = K_3 = 0, \ M^\sigma = M^\tau = 1 \\ &\mathbf{R2}: \ y_1 = \frac{\sqrt{\epsilon}}{2}, \ y_2 = 0, \ y_3 = 0, \ K_2 = K_3, \ K_1 = 0, \ M^\sigma + M^\tau = 1 \end{aligned} \tag{D2}$$

where the RG trajectory around **R2** can flow toward **R1**. Other fixed points includes

$$\mathbf{E1}: \ y_1 = 0, \ y_2 = \frac{\sqrt{\epsilon}}{2}, \ y_3 = 0, \ K_1 = K_3, \ K_2 = 0, \ M^\sigma = 1, \ M^\tau = 0 \tag{D3}$$

and

$$\mathbf{E2}: \ y_1 = 0, \ y_2 = 0, \ y_3 = \frac{\sqrt{\epsilon}}{2}, \ K_1 = K_2, \ K_3 = 0, \ M^\sigma = 0, \ M^\tau = 1 \tag{D4}$$

, and both of the fixed points **E1** and **E2** are unstable and the RG trajectory around them can flow toward **R1** and **R2**. Finally, there is a unstable fixed points

$$\mathbf{E3}: \ y_1 = y_2 = y_3 = 0, \ M^\sigma = M^\tau = 0 \tag{D5}$$

We will ignore this fixed point in the following, since it is the most unstable fixed points.

Among the fixed points listed in the Eq. D2-D5, the fixed point **R1** is the most stable one. However, the fixed point **R1** is actually still not a generic critical point, since there are two relevant directions $\vec{v}_{1,2}$ around it. The first one is:

$$\vec{v}_1 = \frac{1}{2\sqrt{2}}\hat{y}_2 - \frac{1}{2\sqrt{2}}\hat{y}_3 + \hat{M}^\sigma - \hat{M}^\tau \tag{D6}$$

which has the associated eigenvalue scaling dimension $\sqrt{2\epsilon}$ and can flow toward either the orbital KS fixed point:

$$\mathbf{K1}: \ y_2 \to \infty, \ y_1 = y_3 = 0, \ K_1 = K_2 = K_3, \ M^\sigma = 0, \ M^\tau \to \infty$$

or spin KS fixed point:

$$\mathbf{K2}: \ y_3 \to \infty, \ y_1 = y_2 = 0, \ K_1 = K_2 = K_3 = 0, \ M^\sigma \to \infty, \ M^\tau = 0$$

On the other hand, the second relevant direction is(we express each non-vanishing coefficients up to the leading order $\sqrt{\epsilon}$):

$$\vec{v}_2 = \frac{\sqrt{\epsilon}}{2}\hat{y}_1 + \frac{1}{2\sqrt{2}}\hat{y}_2 + \frac{1}{2\sqrt{2}}\hat{y}_3 - \hat{M}^\sigma - \hat{M}^\tau \tag{D7}$$

which has associated scaling dimension $\sqrt{2\epsilon}$(up to the leading order $\sqrt{\epsilon}$) and flows toward either the strong coupling SU(4) Kondo-screened(KS) fixed point

$$\mathbf{K3}: \ y_1, y_2, y_3 \to \infty, \ K_1 = K_2 = K_3 = 0, \ M^\sigma = M^\tau = 0$$

or the spin and orbital Kondo-destroyed(KD) phase

$$\mathbf{G}: \ y_1 = y_2 = y_3 = 0, \ M^\sigma \to \infty, \ M^\tau \to \infty$$

The stability of the strong coupling fixed points **K1**, **K2**, **K3**, and **G** can be studied through the stability matrix $W$ (D1). This analysis shows that the fixed points are stable against other small perturbations and thus characterize the phase of matter. Accordingly, there should be other generic critical points separate these phases. Since there are two relevant directions around **R1**, there should be four generic critical points separating these phase.

Moreover, besides flowing toward to **R1**, **K1**, **K2** and **G**, by exploring the relevant direction around the fixed point **E1** one can also checks that the RG trajectory around it can also flow toward $M^\tau \to \infty$( $M^\sigma \to \infty$), and thus approach to:

$$\mathbf{F1}: \ y_1 = 0, \ y_2 = \frac{\sqrt{\epsilon}}{2}, \ y_3 = 0, \ K_1 = K_2 = K_3 = 0, \ M^\sigma = 1, \ M^\tau \to \infty$$

For the **F1**, except the $\beta$ function $dM^\tau/dl$, other $\beta$ functions remain zero. As a result, **F1** corresponds to a fixed point at the large $M^\tau$ regime. By study the nearby RG trajectory through the matrix $W$ in Eq. (D1), one can conclude that fixed point **F1** actually corresponds to a generic critical point separate the spin and orbital KD phase **G** and the orbital KS phase **K1**.

Similarly the RG trajectory around **E2** can flow toward:

$$\mathbf{F2}: \ y_1 = 0, \ y_2 = 0, \ y_3 = \frac{\sqrt{\epsilon}}{2}, \ K_1 = K_2 = K_3 = 0, \ M^\tau = 1, \ M^\sigma \to \infty$$

which is a generic critical point between the spin and orbital KD phase **G** and the orbital KS phase **K3**.

The whole RG flow structure is summarized in Fig. 5 of the main text, where the blue boxes are the critical points **F1**-**F2** corresponding to the phase transitions from spin and orbital KD phase to spin or orbital KS phases. One can see that the spin and orbital KD phase **G** can transit to different kinds o f strong Kondo coupling fixed points **K1**, **K2**, and **K3**. Note that because the fixed point **R1**, denoted as the red box in Fig. 5, is not a generic but a multi-critical point, the phase transition between spin and orbital KS phase **K3** and spin and orbital KD phase **G** should be a fine-tuned one. Again, since the Kondo screened fixed points **K1**, **K2**, **K3** are stable fixed points, there should be some generic critical points (denoted as the orange boxes **X1** and **X2** in Fig. 5 separating them, even though their exact directions is unknown in this scheme unlike the generic critical point **F1** and **F2**. Based on the whole RG flow structure Fig. 5, the generic phase diagram is sumarrized in Fig. 3(a). Note that in Fig. 5, we neglected the fixed point **R2**, **E1**, **E2** , and **E3** since these fixed points do not influence the RG structure. We present the relative RG flow structure among the fixed points **R1**, **E1**, **F1**, **K1**, and **G** in Fig. (6).

We emphasize that the RG flow structure Fig. 5 is rigorously derived through the matrix $W$ (D1). However, due to the huge number of the coupling constants, it is not easy to visualize the full RG flow structure. In the following, we are going to elaborate these results in a reduced but more transparent and visible way.

### 2. Transition to the SU(4) Kondo-screened phase

To illustrate the transition between the spin and orbital KD phase to the SU(4) KS phase, we choose to scan the RG flow structure by taking $g_{\sigma z} = g_{\tau z} = g$, which corresponds to the trajectory denoted as the arrow (I) in Fig. 3(a).

Since along this direction, the $\beta$ functions (C39) are invariant under $\sigma \leftrightarrow \tau$, one can set $y_2 = y_3 = y$ and

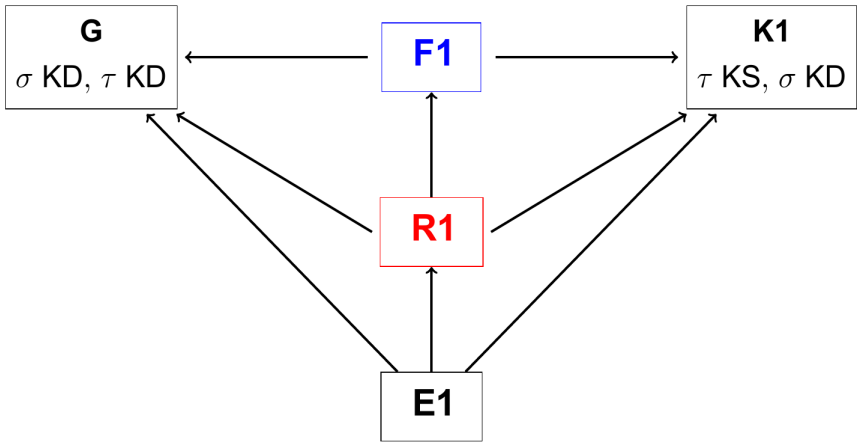


FIG. 6. The relative RG flow structure among the fixed points **R1**, **E1**, **F1**, **K1**, and **G**.

$K_2 = K_3 = K$. The $\beta$ functions (C39) thus can be reduced to:

$$\begin{aligned}
\frac{dy_1}{dl} &= (1 - K_1 - 2M)\, y_1 + 2y^2 \\
\frac{dy}{dl} &= (1 - K - M)\, y + 2y_1 y \\
\frac{dK_1}{dl} &= -2y_1^2\,(2K_1) - 4y^2\,(K_1) \\
\frac{dK}{dl} &= -2y_1^2\,(K_1) - 4y^2\,(2K) + 2y^2\,(K_1) \\
\frac{dM}{dl} &= \left(\epsilon - 4y_1^2 - 4y^2\right) M
\end{aligned} \tag{D8}$$

Note that the fugacity $y_1$ flips both spin and orbital part, while the fugacity $y$ flips only the spin or orbital index. As a result, the $\beta$ functions of $y_1$ and $y$ involve $y^2$ and $y_1 y$, respectively.

From the $\beta$ functions D8, one can see that the coupling constant $K_1$ flows to 0 no matter the initial values, and thus the $\beta$ functions can be further reduced into:

$$\begin{aligned}
\frac{dy_1}{dl} &= (1 - 2M)\, y_1 + 2y^2 \\
\frac{dy}{dl} &= (1 - K - M)\, y + 2y_1 y \\
\frac{dK}{dl} &= -4y^2\,(2K) \\
\frac{dM}{dl} &= \left(\epsilon - 4y_1^2 - 4y^2\right) M
\end{aligned} \tag{D9}$$

and again, $K \to 0$ no matter the initial values, so in the end we derive the reduced $\beta$ functions Eq. (7):

$$\begin{aligned}
\frac{dy_1}{dl} &= (1 - 2M)\, y_1 + 2y^2 \\
\frac{dy}{dl} &= (1 - M)\, y + 2y_1 y \\
\frac{dM}{dl} &= \left(\epsilon - 4y_1^2 - 4y^2\right) M
\end{aligned} \tag{D10}$$

From these reduced $\beta$ functions (D10), we identify the generic critical point $(y_1^*, y^*, M^*) = \left(\frac{-1+\sqrt{1+12\epsilon}}{12}, \frac{\sqrt{-1+12\epsilon+\sqrt{1+12\epsilon}}}{6\sqrt{2}}, \frac{5+\sqrt{1+12\epsilon}}{6}\right) \cong \left(0, \frac{\sqrt{\epsilon}}{2}, 1\right)$ up to the order $\sqrt{\epsilon}$. This critical point corresponds to the critical point **R1** in Fig. 5, and separates the spin and orbital KD phase from the SU(4) KS phase.

### 3. Transition to spin or orbital Kondo-screened phase

Here we aim to illustrate the transition between the spin and orbital KD phase and the spin or orbital KS phase. We firstly focus on the RG trajectory around the critical point **R1** where $g_{\sigma z} = g_{\tau z} = g^*$ between the spin and orbital KD **G** and SU(4) KS phases **K3**.

As mentioned, any small asymmetry between $g_{\tau z}$ and $g_{\sigma z}$ around **R1** actually is relevant in RG sense. Suppose we keep every parameters fixed but just slightly increase the coupling constant $g_{\sigma z}$, that is, $g_{\sigma z} > g_{\tau z} = g^*$, then the RG trajectory will flow toward to $g_{\sigma z} \to \infty$. We can then vary $g_{\tau z}$ to explore the RG trajectory. The corresponding trajectories in the phase diagram are denoted as the arrow (II) in Fig. 3(a). Around this trajectory, according to the $\beta$ functions (C39), $y_1$ and $y_3$ must both flow to 0 and both are irrelevant since $g_{\sigma z} \to \infty$. The $\beta$ functions can thus be reduced into:

$$\begin{aligned}
\frac{dy_2}{dl} &= (1 - K_2 - M^\sigma)\, y_2 \\
\frac{dK_1}{dl} &= -2y_2^2\,(K_1 + K_2 - K_3) \\
\frac{dK_2}{dl} &= -2y_2^2\,(2K_2) \\
\frac{dK_3}{dl} &= -2y_2^2\,(K_3 + K_2 - K_1) \\
\frac{dM^\sigma}{dl} &= \left(\epsilon - 4y_2^2\right) M^\sigma
\end{aligned} \tag{D11}$$

by which one can see that $K_2 \to 0$, and again the $\beta$ functions can be further reduced into:

$$\begin{aligned}
\frac{dy_2}{dl} &= (1 - M^\sigma)\, y_2 \\
\frac{dK_1}{dl} &= -2y_2^2\,(K_1 - K_3) \\
\frac{dK_3}{dl} &= -2y_2^2\,(K_3 - K_1) \\
\frac{dM^\sigma}{dl} &= \left(\epsilon - 4y_2^2\right) M^\sigma
\end{aligned} \tag{D12}$$

From the reduced $\beta$ functions (D12), one can immediately conclude that the $K_1$ and $K_3$ flow to the fixed point $K_1 = K_3 = k_\tau$, where $k_\tau$ is a constant. As a result, the final reduced $\beta$ functions are indeed Eq. (8), from which one can find a generic critical point $(y_2^*, M^{\sigma *}) = \left(\frac{\sqrt{\epsilon}}{2}, 1\right)$ with the scaling dimensions $\frac{1}{2}\sqrt{\epsilon}\left(\sqrt{\epsilon} + \sqrt{8+\epsilon}\right) \cong \sqrt{2\epsilon}$ (up to the order $\sqrt{\epsilon}$) that corresponds to the fixed point **F2** in Fig. 5 and separates the spin and orbital KD phase from the spin KS phase. The RG flow diagram of the reduced $\beta$ functions (8) on the $J_{\sigma\perp} - g_{\sigma z}$ plane is shown in Fig. 7.

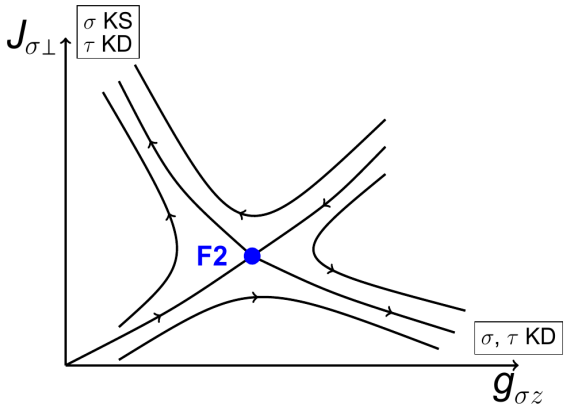


FIG. 7. RG flow diagram of the reduced $\beta$ functions (8) on the $J_{\sigma\perp} - g_{\sigma z}$ plane.

### 4. Transition between spin or orbital KS phase and SU(4) KS phase

Finally, we would like to establish the transition between the spin or orbital KS phase and the SU(4) KS phase, which correspond to the trajectories III in Fig. 3(a). As discussed in the main text, because the strong Kondo coupling fixed points **K1**, **K2**, and **K3** are stable fixed points, there should be other generics critical points, denoted as orange boxes **X1** and **X2**, separating them.

Again, we focus on the RG trajectory around the critical point **R1** where $g_{\sigma z} = g_{\tau z} = g^*$ between the spin and orbital KD **G** and SU(4) KS phases **K3**. If we keep every parameters fixed but just slightly decrease the coupling constant $g_{\sigma z}$, that is, $g_{\sigma z} < g_{\tau z} = g^*$, then the RG trajectory will flow toward to $g_{\sigma z} \to 0$. We can then vary $g_{\tau z}$ to explore the RG trajectory. The corresponding trajectories in the phase diagram are denoted as the arrow (III) in Fig. 3(a). As we will see later, the assumption that $g_{\sigma z} \to 0$ is legitimate since $g_{\sigma z}$ is generally irrelevant around $g_{\sigma z} = 0$.

However, unlike **R1** and **F1**, the real locations of the **X1** is hard to identify directly from the $\beta$ functions (C39). To proceed, we exploit one more property of the critical point **R1**, that is, $y_1 \sim 0$, $y_{2,3} \sim \frac{\sqrt{\epsilon}}{2}$ around **R1**. Near the vicinity of **R1**, one can thus neglect the higher order terms of $\sqrt{\epsilon}$ in the $\beta$ functions (C39). To simplify the analysis, we also set the new variables:

$$\begin{aligned} u_3 &= K_1 + K_2 - K_3 \\ u_2 &= K_1 + K_3 - K_2 \\ u_1 &= K_2 + K_3 - K_1 \end{aligned} \tag{D13}$$

, under all of these conditions the the $\beta$ functions (C39) then become:

$$\begin{aligned} \frac{dy_1}{dl} &= \left(1 - \frac{u_2}{2} - \frac{u_3}{2} - M^\tau\right) y_1 \\ \frac{dy_2}{dl} &= \left(1 - \frac{u_1}{2} - \frac{u_3}{2}\right) y_2 \\ \frac{dy_3}{dl} &= \left(1 - \frac{u_1}{2} - \frac{u_2}{2} - M^\tau\right) y_3 \\ \frac{du_3}{dl} &= -4\left(y_1^2 + y_2^2\right) u_3 \\ \frac{du_2}{dl} &= -4\left(y_1^2 + y_3^2\right) u_2 \\ \frac{du_1}{dl} &= -4\left(y_2^2 + y_3^2\right) u_1 \\ \frac{dM^\sigma}{dl} &= \left(\epsilon - 4y_1^2 - 4y_2^2\right) M^\sigma \\ \frac{dM^\tau}{dl} &= \left(\epsilon - 4y_1^2 - 4y_3^2\right) M^\tau \end{aligned} \tag{D14}$$

by which one can see that $u_1$, $u_2$, and $u_3$ are generally irrelevant and flow to zero, and thus the resulting $\beta$ functions are

$$\begin{aligned} \frac{dy_1}{dl} &= \left(1 - M^\tau\right) y_1 \\ \frac{dy_2}{dl} &= y_2 \\ \frac{dy_3}{dl} &= \left(1 - M^\tau\right) y_3 \\ \frac{dM^\sigma}{dl} &= \left(\epsilon - 4y_1^2 - 4y_2^2\right) M^\sigma \\ \frac{dM^\tau}{dl} &= \left(\epsilon - 4y_1^2 - 4y_3^2\right) M^\tau \end{aligned} \tag{D15}$$

From the reduced $\beta$ functions (D15), one can immediately conclude that $y_2 \to \infty$, and thus $M^\sigma$ is indeed irrelevant

around $M^\sigma \to 0$. The final reduced $\beta$ functions are

$$\begin{aligned}\frac{dy_1}{dl} &= (1-M^\tau)\, y_1 \\ \frac{dy_3}{dl} &= (1-M^\tau)\, y_3 \\ \frac{dM^\tau}{dl} &= \left(\epsilon - 4y_1^2 - 4y_3^2\right) M^\tau\end{aligned} \tag{D16}$$

from which one can identify a critical line $(y_1^*, y_3^*, M^{\tau *}) = \left(a, \frac{\sqrt{\epsilon-4a^2}}{2}, 1\right)$ where $a$ is a constant, which has one relevant direction with the associated scaling dimension $\sqrt{2\epsilon}$ and separates the spin and orbital KS phase from the spin KS phase and corresponds to the critical point **X1** in Fig. 5. The RG flow diagram of reduced $\beta$ functions (D16) is plotted in Fig (8). By a parallel analysis, the transition between the spin and orbital KS phase and the orbital KS phase can also be established.

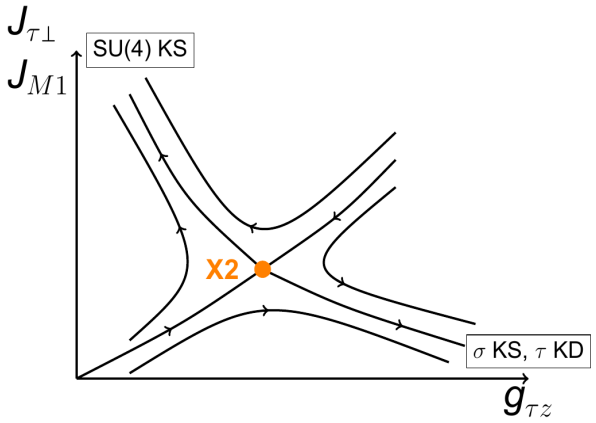


FIG. 8. RG flow diagram of the reduced $\beta$ functions (D16).

## Appendix E: RG analysis with a small cross-product term $g_m$

In this section, we aim to study the stability of the phase diagram Fig. 3(a) under a small cross-product term $g_m\left(\sigma_z \otimes \tau_z\right)\phi_m$ through RG analysis. In other words, we derive the $\beta$ functions of the Bose-Fermi-Kondo model $H_{BFK}$ where the coupling with the bosonic bath is modified as:

$$H_{\mathrm{BK}} = g_{\sigma z}\sigma_z\phi_{\sigma z} + g_{\tau z}\tau_z\phi_{\tau z} + g_m\left(\sigma_z \otimes \tau_z\right)\phi_m \tag{E1}$$

After mapping the model into a Coulomb-gas type action, one can derive the $\beta$ functions:

$$\begin{aligned}
\frac{dy_1}{dl} &= \left(1-K_1-M^\sigma-M^\tau\right)y_1+2y_2y_3\\
\frac{dy_2}{dl} &= \left(1-K_2-M^\sigma-M^m\right)y_2+2y_1y_3\\
\frac{dy_3}{dl} &= \left(1-K_3-M^\tau-M^m\right)y_3+2y_1y_2\\
\frac{dK_1}{dl} &= -2y_1^2\left(2K_1\right)-2y_2^2\left(K_1+K_2-K_3\right)-2y_3^2\left(K_1+K_3-K_2\right)\\
\frac{dK_2}{dl} &= -2y_1^2\left(K_2+K_1-K_3\right)-2y_2^2\left(2K_2\right)-2y_3^2\left(K_2+K_3-K_1\right)\\
\frac{dK_3}{dl} &= -2y_1^2\left(K_3+K_1-K_2\right)-2y_2^2\left(K_3+K_2-K_1\right)-2y_3^2\left(2K_3\right)\\
\frac{dM^\sigma}{dl} &= \left(\epsilon-4y_1^2-4y_2^2\right)M^\sigma\\
\frac{dM^\tau}{dl} &= \left(\epsilon-4y_1^2-4y_3^2\right)M^\tau\\
\frac{dM^m}{dl} &= \left(\epsilon-4y_2^2-4y_3^2\right)M^m
\end{aligned} \tag{E2}$$

where $M^m=\Gamma\left(\epsilon\right)g_m^2$.

Since our purpose is only to study the stability of the phase diagram Fig. 3(a) under small $g_m$, we only need to check the $\beta$ function:

$$\frac{dM^m}{dl}=\left(\epsilon-4y_2^2-4y_3^2\right)M^m \tag{E3}$$

by which one can see only the spin and orbital KD fixed point **G** is unstable against a small $M^m$(and thus $g_m$), while the KS fixed point **K3**, spin or orbital KS fixed points **K2** and **K1**, the generic critical points **F1**, **F2**, and the multi-critical point **R1**, are stable against a weak coupling constant $g_m$.

As a result, the structure of the the phase diagram Fig. 3(a) remains unchanged, except now the spin and orbital KD phase correspond to the fixed point:

$$\textbf{G'}:\ y_1=y_2=y_3=0,\ M^\sigma\to\infty,\ M^\tau\to\infty,\ M^m\to\infty$$

instead of **G**.


[1] S. Paschen and Q. Si *Quantum phases driven by strong correlations*, Nature Review Physics, in press; arXiv:2009.03602.

[2] G. R. Stewart, *Non-Fermi-liquid behavior in d- and f-electron metals*, Rev. Mod. Phys. **73**, 797?855 (2001).

[3] P. Coleman and A. J. Schofield, *Quantum Criticality*, Nature **433**, 226-229 (2005).

[4] S. Kirchner, S. Paschen, Q. Y. Chen, S. Wirth, D. L. Feng, J. D. Thompson, and Q. Si, *Colloquium: Heavy-electron quantum criticality and single-particle spectroscopy*, Rev. Mod. Phys. **92**, 011002 (2020).

[5] A. C. Hewson *The Kondo Problem to Heavy Fermions*, Cambridge Studies in Magnetism (Cambridge Univ. Press, 1993).

[6] Q. Si, S. Rabello, K. Ingersent, and J. Smith *Locally critical quantum phase transitions in strongly correlated metals*, Nature **413**, 804 (2001).

[7] P. Coleman, C. Pépin, C., Q. Si, and R. Ramazashvili, *How do Fermi liquids get heavy and die?* J. Phys. Condens. Matter **13**, R723-R738 (2001).

[8] T. Senthil, M. Vojta, and S. Sachdev, *Weak magnetism and non-Fermi liquids near heavy-fermion critical points*, Phys. Rev. B **69**, 035111 (2004).

[9] A. Schröder, G. Aeppli, R. Coldea, M. Adams, O. Stockert, H. v. Löhneysen, E. Bucher, R. Ramazashvili, and P. Coleman, *Onset of antiferromagnetism in heavy-fermion metals*, Nature **407**, 351 (2000).

[10] S. Paschen, T. Lühmann, S. Wirth, P. Gegenwart, O. Trovarelli, C. Geibel, F. Steglich, P. Coleman, and Q. Si, *Hall-effect evolution across a heavy-fermion quantum critical point*, Nature **432**, 881 (2004).

[11] H. Shishido, R. Settai, H. Harima, and Y. Onuki, *A drastic change of the Fermi surface at a critical pressure in $CeRhIn_5$: dHvA study under pressure*, J. Phys. Soc. Jpn.

**74**, 1103 (2005).

[12] T. Park, V. A. Sidorov, F. Ronning, J.-X. Zhu, Y. Tokiwa, H. Lee, E. D. Bauer, R. Movshovich, J. L. Sarrao, and J. D. Thompson, *Isotropic quantum scattering and unconventional superconductivity*, Nature **456**, 366 (2008).

[13] L. Prochaska, X. Li, D. C. MacFarland, A. M. Andrews, M. Bonta, E. F. Bianco, S. Yazdi, W. Schrenk, H. Detz, A. Limbeck, Q. Si, E. Ringe, G. Strasser, J. Kono, and S. Paschen, *Singular charge fluctuations at a magnetic quantum critical point*, Science **367**, 285 (2020).

[14] A. Patri, I. Khait, and Y. B. Kim, *Emergent non-Fermi-liquid phenomena in multipolar quantum impurity systems*, Phys. Rev. Research **2**, 013257 (2020).

[15] A. Patri, and Y. B. Kim, *Critical Theory of Non-Fermi Liquid Fixed Point in Multipolar Kondo Problem*, Phys. Rev. X **10**, 041021 (2020).

[16] H.-H. Lai, E. Nica, W.-J. Hu, S.-S. Gong, S. Paschen, and Q. Si, *Kondo Destruction and Multipolar Order–Implications for Heavy Fermion Quantum Criticality*, arXiv:1807.09258.

[17] J. S. Van Dyke, G. H. Zhang, and R. Flint, *Field-induced ferrohastatic phase in cubic non-Kramers doublet systems*, Phys. Rev. B **100**, 205122 (2019).

[18] G. H. Zhang, J. S. Van Dyke, and R. Flint *Cubic hastatic order in the two-channel Kondo-Heisenberg model*, Phys. Rev. B **98**, 235143 (2018).

[19] C. J. Bolech and N. Andrei, *Solution of the multichannel Anderson impurity model: Ground state and thermodynamics*, Phys. Rev. B **71**, 205104 (2005).

[20] C. J. Bolech and N. Andrei *Solution of the Two-Channel Anderson Impurity Model: Implications for the Heavy Fermion $UBe_{13}$*, Phys. Rev. Lett. **88**, 237206 (2002).

[21] D. L. Cox and A. Zawadowski, *Exotic Kondo Effects in Metals: Magnetic Ions in a Crystalline Electric Field and Tunnelling Centres*, Adv. Phys. **47**, 599 (1998).

[22] Q. Si, R. Yu, and E. Abrahams, *High-temperature superconductivity in iron pnictides and chalcogenides*, Nat. Rev. Mater. **1**, 16017 (2016).

[23] C. Aron, and G. Kotliar, *Analytic theory of hund's metals: A renormalization group perspective*, Phys. Rev. B **91**, 041110 (2015).

[24] E. Walter, K. Stadler, S.-S. B. Lee, Wang, G. Kotliar, A. Weichselbaum, and J. von Delf, *Uncovering Non-Fermi-Liquid Behavior in Hund Metals: Conformal Field Theory Analysis of an SU(2)×SU(3) Spin-Orbital Kondo Model*, Phys. Rev. X **10**, 031052 (2020).

[25] T. T. Ong and P. Coleman, *Local Quantum Criticality of an Iron-Pnictide Tetrahedron*, Phys. Rev. Lett. **108**, 107201 (2012).

[26] Y. Nishida, *SU(3) Orbital Kondo Effect with Ultracold Atoms*, Phys. Rev. Lett. **111**, 135301 (2013).

[27] K. Le Hur, and P. Simon, *Smearing of charge fluctuations in a grain by spin-flip assisted tunneling* , Phys. Rev. B **67**, 201308 (2003).

[28] R. M. Potok, I. G. Rau, H. Shtrikman, Y. Oreg, and D. Goldhaber-Gordon, *Observation of the two-channel Kondo effect*, Nature **446**, 167-171 (2007).

[29] A. Mitchell, A. Liberman, E. Sela, and I. Affleck *SO(5) non-Fermi liquid in a Coulomb box device*, arXiv:2009.12700.

[30] A. Horvat, R. Zitko, and J. Mravlje, *Low-energy physics of three-orbital impurity model with Kanamori interaction*, Phys. Rev. B **94**, 165140 (2016).

[31] J. G. Rau and H.-Y. Kee, *Symmetry breaking via hybridization with conduction electrons in frustrated Kondo lattices*, Phys. Rev. B **89**, 075128 (2014).

[32] P. Coleman, L. B. Ioffe, and A. M. Tsvelik, *Simple formulation of the two-channel Kondo model*, Phys. Rev. B **52**, 6611 (1995).

[33] I. Affleck and A. W. W Ludwig, *Critical theory of overscreened Kondo fixed points*, Nucl. Phys. B**360**, 641(1991).

[34] S. Paschen and J. J. Larrea, *Ordered Phases and Quantum Criticality in Cubic Heavy Fermion Compounds*, J. Phys. Soc. Jpn **83**, 061004 (2014).

[35] A. Sakai and S. Nakatsuji *Kondo effects and multipolar order in the cubic $PrTr_2Al_{20}$ (Tr=Ti, V)* , J. Phys. Soc. Jpn. **80**, 063701 (2011).

[36] Y. Shimura, M. Tsujimoto, B. Zeng, L. Balicas, A. Sakai, and S. Nakatsuji, *Field-induced quadrupolar quantum criticality in $PrV_2Al_{20}$*, Phys. Rev. B **91**, 241102(R) (2015).

[37] A. McCollam, B. Andraka, S. R. Julian, *Fermi volume as a probe of hidden order*, Phys. Rev. B **88**, 075102 (2013).

[38] E. D. Bauer, N. A. Frederick, P. C. Ho, V. S. Zapf, M. B. Maple, *Superconductivity and heavy fermion behavior in $PrOs_4Sb_{12}$*, Phys. Rev. B **65**, 100506 (2002).

[39] E. W. Rosenberg, J.-H. Chu, J. P. C. Ruff, A. T. Hristov, and I. R. Fisher, *Divergence of the quadrupole-strain susceptibility of the electronic nematic system $YbRu_2Ge_2$*, Proc. Natl. Acad. Sci. U.S.A **116**, 7232-7237 (2019).

[40] H. S. Jeevan, C. Geibel, and Z. Hossain, *Quasiquartet crystal-electric-field ground state with possible quadrupolar ordering in the tetragonal compound $YbRu_2Ge_2$*, Phys Rev B **73**, 020407 (2006).

[41] V. Martelli, A. Cai, E. M. Nica, M. Taupin, A. Prokofiev, C.-C. Liu, H.-H. Lai, R. Yu, K. Ingersent, R. Küchler, A. M. Strydom, D. Geiger, J. Haenel, J. Larrea, Q. Si, and S. Paschen *Sequential localization of a complex electron fluid*, Proc. Natl. Acad. Sci. U.S.A **116**, 17701 (2019).

[42] J. Custers, K. Lorenzer, M. Müller, A. Prokofiev, A. Sidorenko, H. Winkler, A. M. Strydom, Y. Shimura, T. Sakakibara, R. Yu, Q. Si, and S. Paschen *Destruction of the Kondo effect in the cubic heavy-fermion compound $Ce_3Pd_{20}Si_6$*, Nature Materials **11**, 189 (2012).

[43] R. Shiina, H. Shiba, and P. Thalmeier, *Magnetic-Field Effects on Quadrupolar Ordering in a $\Gamma_8$-Quartet System $CeB_6$*, J. Phys. Soc. Jpn. **66**, 1741 (1997).

[44] K.-A. Lorenzer, *Quantum critical behaviour in cubic heavy-fermion compounds*, PhD thesis, Vienna University of Technology, (2012).

[45] Q. Si and J. L. Smith, *Kosterlitz-Thouless Transition and Short Range Spatial Correlations in an Extended Hubbard Model*, Phys. Rev. Lett. **77**, 3391 (1996).

[46] J. Smith, and Q. Si, *Spatial correlations in dynamical mean-field theory*, Phys. Rev. B **61**, 5184 (2000).

[47] R. Chitra, G. Kotliar, *Effective-action approach to strongly correlated fermion systems*, Phys. Rev. B **63**, 115110 (2001).

[48] L. Zhu, and Q. Si, *Critical local-moment fluctuations in the bose-fermi kondo model*, Phys. Rev. Lett. **66**, 024426 (2002).

[49] Q. Si, and J. Smith, *Kosterlitz-Thouless Transition and Short Range Spatial Correlations in an Extended Hubbard Model* , Phys. Rev. Lett. **77**, 3391 (1996).

[50] J. Smith, and Q. Si *Non-Fermi liquids in the two-band extended Hubbard model* , Europhys. Lett. **45**, 228 (1999).

[51] Here we ignore a unstable fixed point $(y_1^*, y^*, M^*) = \left(\frac{\sqrt{\epsilon}}{2}, 0, \frac{1}{2}\right)$, because the RG trajactories around it can flow

toward the generic critical point $\left(0, \frac{\sqrt{\epsilon}}{2}, 1\right)$, it does not influence the structure of the RG flow diagram (3(b)).

[52] S. Chakravarty and J. E. Hirsch, *Approximate mapping of the two-impurity symmetric Anderson model in the local-moment regime to a classical problem* , Phys. Rev. B **25**, 3273 (1982).

[53] J. Cardy, *One-dimensional models with* $1/r^2$ *interactions*, J. Phys. A: Math. Gen. **14**, 1407 (1981).

[54] Q. Si and G. Kotliar, *Metallic non-Fermi-liquid phases of an extended Hubbard model in infinite dimensions*, Phys. Rev. B **48**, 13881 (1993).